

CAPITAL UNIVERSITY OF SCIENCE AND
TECHNOLOGY, ISLAMABAD



A Mixture Theory Approach for Modeling Fluid Flow Through Deformable Porous Tissues

by

Aftab Ahmed

A thesis submitted in partial fulfillment for the
degree of Doctor of Philosophy

in the

Faculty of Computing

Department of Mathematics

2018

A Mixture Theory Approach for Modeling Fluid Flow Through Deformable Porous Tissues

By

Aftab Ahmed

(DMT143007)

Foreign Evaluator 1

Dr. Nicholas R. Gewecke, Assistant Professor
Dalton State University, Dalton, Georgia, USA

Foreign Evaluator 2

Dr. Daniel M. Anderson, Professor
George Mason University, Fairfax, Virginia, USA

Dr. Javed Iqbal Siddique

(Thesis Supervisor)

Dr. Muhammad Sagheer

(Head, Department of Mathematics)

Dr. Muhammad Abdul Qadir

(Dean, Faculty of Computing)

DEPARTMENT OF MATHEMATICS
CAPITAL UNIVERSITY OF SCIENCE AND TECHNOLOGY
ISLAMABAD

2018

Copyright © 2018 by Aftab Ahmed

All rights reserved. No part of this thesis may be reproduced, distributed, or transmitted in any form or by any means, including photocopying, recording, or other electronic or mechanical methods, by any information storage and retrieval system without the prior written permission of the author.

This dissertation is dedicated to my parents and family.

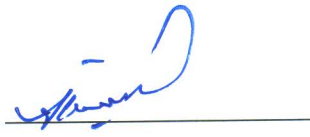


**CAPITAL UNIVERSITY OF SCIENCE & TECHNOLOGY
ISLAMABAD**

Expressway, Kahuta Road, Zone-V, Islamabad
Phone: +92-51-111-555-666 Fax: +92-51-4486705
Email: info@cust.edu.pk Website: <https://www.cust.edu.pk>

CERTIFICATE OF APPROVAL

This is to certify that the research work presented in the thesis, entitled “**A Mixture Theory Approach for Modeling Fluid Flow Through Deformable Porous Tissues**” was conducted under the supervision of **Dr. Javed Iqbal Siddiqui**. No part of this thesis has been submitted anywhere else for any other degree. This thesis is submitted to the **Department of Mathematics, Capital University of Science and Technology** in partial fulfillment of the requirements for the degree of Doctor in Philosophy in the field of **Mathematics**. The open defence of the thesis was conducted on **02 August, 2018**.

Student Name : Mr. Aftab Ahmed (DMT143007) 

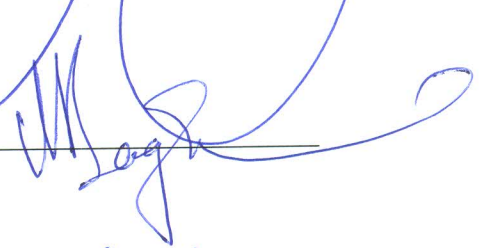
The Examining Committee unanimously agrees to award PhD degree in the mentioned field.

Examination Committee :

- (a) External Examiner 1: Dr. Abdul Rahman, Professor
University of Sargodha,
Gujranwala Campus
- (b) External Examiner 2: Dr. Anwar Hussain,
Associate Professor
CEME, NUST, Islamabad
- (c) Internal Examiner : Dr. Muhammad Sagheer
Professor
Capital University of Science &
Technology, Islamabad



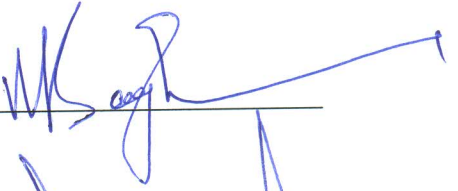




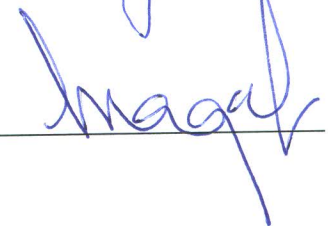
Supervisor Name : Dr. Javed Iqbal Siddiqui
Associate Professor
Capital University of Science &
Technology, Islamabad



Name of HoD : Dr. Muhammad Sagheer
Professor
Capital University of Science &
Technology, Islamabad



Name of Dean : Dr. Muhammad Abdul Qadir
Professor
Capital University of Science &
Technology, Islamabad



AUTHOR'S DECLARATION

I, **Mr. Aftab Ahmed (Registration No. DMT143007)**, hereby state that my PhD thesis titled, '**A Mixture Theory Approach for Modeling Fluid Flow Through Deformable Porous Tissues**' is my own work and has not been submitted previously by me for taking any degree from Capital University of Science and Technology, Islamabad or anywhere else in the country/ world.

At any time, if my statement is found to be incorrect even after my graduation, the University has the right to withdraw my PhD Degree.



(Mr. Aftab Ahmed)

Dated: August 02, 2018

Registration No : DMT143007

PLAGIARISM UNDERTAKING

I solemnly declare that research work presented in the thesis titled “**A Mixture Theory Approach for Modeling Fluid Flow Through Deformable Porous Tissues**” is solely my research work with no significant contribution from any other person. Small contribution/ help wherever taken has been duly acknowledged and that complete thesis has been written by me.

I understand the zero tolerance policy of the HEC and Capital University of Science and Technology towards plagiarism. Therefore, I as an author of the above titled thesis declare that no portion of my thesis has been plagiarized and any material used as reference is properly referred/ cited.

I undertake that if I am found guilty of any formal plagiarism in the above titled thesis even after award of PhD Degree, the University reserves the right to withdraw/ revoke my PhD degree and that HEC and the University have the right to publish my name on the HEC/ University Website on which names of students are placed who submitted plagiarized thesis.

Dated: 02 August, 2018



(Mr. Aftab Ahmed)

Registration No. DMT143007

List of Publications

It is certified that following publication(s) have been made out of the research work that has been carried out for this thesis:-

1. **A. Ahmed**, J. I. Siddique, and A. Mahmood, “Non-Newtonian flow-induced deformation from pressurized cavities in absorbing porous tissues,” *Computer Methods in Biomechanics and Biomedical Engineering*, vol. 20, pp. 1464-1473, 2017.
2. J. I. Siddique, **A. Ahmed**, A. Aziz, and C. M. Khaliq “A review of mixture theory for deformable porous media and applications,” *Applied Sciences*, vol. 7, pp. 917-931, 2017.
3. **A. Ahmed** and J. I. Siddique, “Ion-induced deformation of articular cartilage with strain-dependent nonlinear permeability and MHD effects,” *Journal of Porous Media*, accepted, 2018.
4. J. I. Siddique and **A. Ahmed**, “The effect of magnetic field on flow-induced deformation in absorbing porous tissues,” *Mathematical Biosciences and Engineering*, under review, 2018.

Aftab Ahmed

(DMT143007)

Acknowledgements

First and foremost I owe my profound thanks to “Almighty Allah”, Who endowed me with the potential and ability to make solid contribution to the already existing ocean of scientific knowledge. The author invokes peace and blessings upon the last Prophet Muhammad (PBUH), Who is forever a source of guidance and knowledge for humanity as a whole.

I would like to express my deepest gratitude to my supervisor, Prof. Dr. Javed Iqbal Siddique, for his invaluable suggestions, continuous encouragement and constructive criticism during both the period of research and writing of this thesis. He has always given patiently of his time and tolerated my untimely disturbance. It has been a privilege to learn from him and be guided throughout the last three years. His help in introducing me to other members of the scientific community is and will continue to be invaluable.

I express my sincere gratitude to Prof. Dr. Muhammad Sagheer, head of mathematics department, for all his encouragement and support and for providing necessary facilities for the research work. I always found him welcoming and concerned for solving the problems of students. I am also very thankful to Dr. Shafqat Hussain for his discussion and assistance regarding softwares and codes. I would like to extend my appreciation to Dr. Rashid Ali, Dr. Abdur Rehman Kashif and the rest of the staff of mathematics department for their moral support during my stay. I take this opportunity to thank my M. Phil. supervisor Dr. Qari Naseer Ahmed (Late), may his soul rest in peace, for guiding me on the path of research. I am also very grateful to all my teachers right from the beginning who enabled me to reach this level of academic qualification.

I feel extremely indebted to my affectionate and beloved parents for all their sacrifices, tireless support and prayers throughout my academic career, without which I would not be able to reach at this stage. Especially my mother, may she lives long, has always been a source of great inspiration and strength for me. I am incredibly thankful for the lasting support of my brothers and sisters, especially

my elder brother Khalid Mehmood, who has always been the first to turn up, when I needed the most. Moreover, special thanks goes to all other parental and in-law family members for their indispensable backing and encouragement. I wish to thank all my friends, colleagues and fellows (Usman, Umair, Azhar, Sohail, Naveed, Yasir, Bilal, etc) for constant support, love and wonderful company.

Last but by no means least, I would like to express my warmest gratitude to my wife and sons Muhammad Abdul Nafay and Muhammad Abdullah for all their love and care. They have always encouraged me and tolerated my academic activities at the cost of family and social life. In addition to this, her assistance and information regarding the biological terms related to my work is also greatly acknowledged.

Abstract

In this thesis, the problems of flow and ion-induced deformation of soft porous biological tissues have been examined by using continuum mixture theory approach. In particular, we focus on the tissue deformation due to non-Newtonian fluid and externally applied magnetic field. In this regard, we first analyze the problem of non-Newtonian flow-induced deformation from pressurized cavities in absorbing porous tissues. Specifically, a model with a spherical cavity embedded in an infinite porous medium is used to find fluid pressure and solid displacement in the tissue as a function of non-dimensional radial distance and time. The governing nonlinear equations have been solved numerically to highlight effects of various emerging parameters. Furthermore, based on the geometry of the previous problem, the effect of the externally applied magnetic field on flow-induced deformation of absorbing porous tissues is investigated. A biphasic mixture theory approach has been used to develop a mathematical model. The governing dimensionless equations for fluid pressure and solid displacement have been solved numerically using the method of lines approach and the trapezoidal rule, respectively. The effect of magnetic parameter on fluid pressure and solid displacement is illustrated graphically. Finally, the problem of ion-induced deformation of articular cartilage with strain-dependent nonlinear permeability and magnetohydrodynamic effects is presented. The governing set of coupled partial differential equations are non-dimensionalized using suitable dimensionless variables. Analytical solutions are provided for the constant permeability case whereas for the nonlinear permeability case the displacement equation is solved numerically using the method of lines technique. The influence of magnetic and permeability parameter on solid displacement and fluid pressure is illustrated graphically. In some cases, a graphical comparison to the previously reported literature is also presented.

Contents

Author's Declaration	v
Plagiarism Undertaking	vi
List of Publications	vii
Acknowledgements	viii
Abstract	x
List of Figures	xiii
List of Tables	xiv
Symbols	xv
1 Introduction	1
1.1 Historical Background	2
1.2 Thesis Outline	6
2 Preliminaries	9
2.1 Introduction	9
2.2 Porous Material	9
2.3 Porosity	10
2.4 Darcy's Law	11
2.5 Permeability	12
2.6 Fluid Classification	12
2.6.1 Newtonian Fluid	13
2.6.2 Non-Newtonian Fluid	13
2.7 Magnetohydrodynamics	15
2.8 Biological Tissue	15
2.9 Mixture Theory: Kinematics and Balance Laws	17
2.10 Numerical Method and Matlab Solvers	19
2.10.1 Method of Lines	20
2.10.2 bvp4c	22

2.10.3 pdepe	22
3 Non-Newtonian Flow-Induced Deformation From Pressurized Cavities in Absorbing Porous Tissues	24
3.1 Introduction	24
3.2 Mathematical Formulation	25
3.3 Initial and Boundary Conditions	33
3.4 Results and Discussion	35
3.5 Conclusion	42
4 Application of Magnetic Field to Flow Induced-Deformation in Absorbing Porous Tissues	44
4.1 Introduction	44
4.2 Mathematical Formulation	45
4.3 Solution Methodology	52
4.4 Results and Discussion	54
4.5 Concluding Remarks	59
5 Ion-Induced Deformation of Articular Cartilage with Strain-Dependent Nonlinear Permeability and MHD Effects	61
5.1 Introduction	61
5.2 Mathematical Modeling	62
5.3 Solution Procedure	68
5.4 Results and Discussion	71
5.4.1 Ion concentration profile	71
5.4.2 Influence of magnetic parameter	72
5.4.3 Influence of permeability parameter	74
5.5 Concluding Remarks	76
6 Conclusion and Future Work	78
6.1 Conclusion	78
6.2 Future Work	80
A MHD Equations for a Biphasic Mixture	91

List of Figures

2.1	Basic schematic of a porous material	10
2.2	Relation between shear rate and viscosity	14
2.3	Types of tissue	16
2.4	A comparison between the exact and MOL solution	21
3.1	Schematic of power-law fluid flow through a spherical cavity	26
3.2	Power-law fluid pressure vs time	36
3.3	Pressure vs radius for various n	37
3.4	Displacement vs radius for various n	38
3.5	Steady-state pressure and displacement vs radius for various ξ	39
3.6	Steady-state pressure and displacement vs radius for various n	40
3.7	Pressure and displacement gradient vs radius for various n	41
3.8	Pressure-dependent permeability vs radius for various n	42
4.1	Schematic of MHD fluid flow through a spherical cavity	46
4.2	A comparison between the exact and MOL solution for $p(r, t)$	54
4.3	Fluid pressure vs time for various $g(t)$	55
4.4	Fluid pressure vs radius for various M	56
4.5	Solid displacement vs radius for various M	57
4.6	Pressure-dependent permeability vs radius for various M	58
4.7	Fluid pressure vs radius for various ω	59
4.8	Solid displacement vs radius for various ω	59
5.1	Schematic of cartilage sample under salt bath and magnetic field	62
5.2	Ion concentration vs distance for various times	72
5.3	Solid displacement vs distance for various M and t	73
5.4	Fluid pressure vs distance for various M and t	74
5.5	Strain-dependent permeability vs distance for various M	74
5.6	Solid displacement vs distance for various m	75
5.7	Pressure gradient vs distance for various m	76

List of Tables

2.1	Maximum absolute error between the exact and MOL solution . . .	22
-----	---	----

Symbols

V_E	volume of empty space	V_T	volume of total space
ϕ	porosity	v	fluid velocity
κ	permeability	μ	dynamic viscosity
ΔP	applied pressure difference	Δh	porous material thickness
τ	shear stress	Q^*	flow rate
ν	kinematic viscosity	ρ	density
K^*	flow consistency index	n	power law index
A	specific area of porous material	\mathbf{x}	position vector
\mathbf{X}	particle position in reference configuration	ρ^η	density of η phase
ϕ^η	porosity of η phase	\mathbf{v}^η	velocity of η phase
\mathbf{F}^η	deformation gradient of η phase	t	time
\mathbf{u}^η	diffusion velocity of η phase	\mathbf{T}^η	stress tensor of η phase
\mathbf{b}^η	body force of η phase	K	drag coefficient
dm^η	mass of η phase	dV^η	small volume of η phase
dV	total volume of tissue	ρ_T^η	actual density of η phase
ρ^s	density of solid phase	ρ^ℓ	density of fluid phase
ϕ^s	porosity of solid phase	ϕ^ℓ	porosity of fluid phase
β	proportionality constant	p	fluid pressure in tissue
ρ_T^ℓ	actual density of fluid phase	$\boldsymbol{\pi}^\eta$	drag force on η phase
\mathbf{I}	identity tensor	$\boldsymbol{\sigma}^\eta$	stress of η phase
$\boldsymbol{\sigma}^s$	solid stress	$\boldsymbol{\pi}^s$	drag force on solid phase
$\boldsymbol{\pi}^\ell$	drag force on fluid phase	σ_{rr}	stress component in r direction
$\sigma_{\theta\theta}$	stress component in θ direction	$\sigma_{\phi\phi}$	stress component in ϕ direction

\mathbf{v}^f	velocity of fluid phase	\mathbf{v}^s	velocity of solid phase
\mathbf{u}	solid displacement vector	u	solid displacement component
λ, μ	Lamé stress constants	r	radial distance
H_a	aggregate modulus of solid	v_r	composite velocity component
m	permeability parameter	α	a dimensionless parameter
δ	a dimensionless parameter	ω	a dimensionless parameter
γ	a dimensionless parameter	R	a dimensionless parameter
$f(r)$	initial applied pressure	σ_0	electric conductivity of fluid
ξ	absorption parameter	$g(t)$	applied pressure
v^f	component of fluid velocity	v^s	component of solid velocity
$a(t)$	radius of spherical cavity	\mathbf{G}	left Cauchy-Green tensor
ϕ_0^s	initial solid volume fraction	ϕ_0^ℓ	initial fluid volume fraction
α_0	ratio of ϕ_0^s to ϕ_0^ℓ	κ_0	undeformed permeability
M	dimensionless magnetic parameter	$\bar{\lambda}$	dimensionless constant
$erfc(\cdot)$	complementary error function	$\Gamma(\cdot)$	gamma function
C	molar concentration of salt	C_0	step rise in salt concentration
D	diffusion coefficient of salt	\mathbf{e}	infinitesimal strain tensor
e	trace of strain tensor	h	thickness of cartilage sample
w	width of cartilage sample	l	length of cartilage sample
$H(t)$	unit step function	x	coordinate in thickness direction
y	coordinate in width direction	z	coordinate in length direction
ψ	solid to fluid volume ratio	\mathbf{J}	current density
ψ_c	coefficient of chemical contraction	\mathbf{E}	electric field
B_0	uniform magnetic flux	μ_c	permeability of free space
\mathbf{B}	total magnetic field	\mathbf{b}	induced magnetic field
\mathbf{B}_0	imposed magnetic field	q	fluid flux
p_0	initial pressure	Q	a dimensionless parameter

Chapter 1

Introduction

The aim of this dissertation is to investigate the deformation of soft biological tissues due to fluid flow or ion imbalance using continuum mixture theory approach. The tissues are modeled as nonlinear deformable porous media comprised of a solid and a fluid phase. Apart from mixture theory for modeling multiphase systems, many other theoretical frameworks such as finite elasticity, viscoelasticity, growth and remodeling, thermomechanics and membrane theory were devised to study the incredibly complex behaviors of soft tissues. A brief description of each of these theories was given by Humphrey [1] in an excellent review paper on continuum biomechanics of soft biological tissues mentioning the past successes and identifying open problems for future research. He felt the need for new and comprehensive theoretical frameworks, accurate mathematical models and efficient computational approaches for modeling biological tissues for an improved and better health-care delivery. Moreover, while describing other open problems in biomechanics, Humphrey also emphasized the need to further explore the solid-fluid interaction in living organisms such as removal of waste products by the kidney, bladder and urinary tract, gas exchange process in lungs and pumping of the blood by the heart, etc. Moreover, the deformational behavior of soft biological tissues such as articular cartilage, skin, and arterial wall **has** been investigated extensively to understand the solid-fluid interaction in biological systems. The phenomenon of solid-fluid interaction occurs in many branches of science ranging

from soil mechanics to biomechanics. Therefore, motivated by the importance of coupling between solid and fluid in a physiological system such as flow from an injection site into a tissue and permeation of fluid through soft tissues, the goal of the present research is to gain a better understanding of the dynamical and mechanical processes involved in solid-fluid interaction in porous tissues. Although, accurate and direct biological modeling is avoided here, nevertheless, this study serves as a reasonable platform for gaining an insight into the deformation phenomena of soft tissues involving a variety of fluid models along with different geometries.

The mathematical models developed in this thesis are based on continuum mixture theory. It is thus important to furnish a historical background of the theory along with its development and applications in biomechanics. However, for applications of this theory in some other scientific fields, the reader is referred to a recent review article by Siddique *et al.* [2]. This is followed by a thesis outline in Section 1.2 giving a brief description of each chapter in this thesis.

1.1 Historical Background

The deformation of a porous material changes the properties such as porosity and permeability of the material, which consequently affects the passage of fluid through the material. This process develops a complex coupling among constituents of the mixture. This type of phenomenon exists in various biological and industrial applications where mathematical modeling is usually done using continuum mixture theory. In mixture theory, individual components of the mixture are treated as superimposing continua so that each point in the mixture is occupied simultaneously by a material point of each constituent. This assumption, although physically inaccurate, is necessary so that the quantities used to describe deformation are continuous and differentiable. The literature that laid down the foundations of mixture theory were presented by Fick [3], Stefan [4] and Darcy [5] in the nineteenth century. This was later improved by Truesdell and

Noll [6], where he included the principles of continuum mechanics and proposed balance equations appropriate to mixtures irrespective of their constitution. The theory developed by Truesdell was named as a mechanical basis for diffusion in which mass and momentum balance laws for the mixture constituents were postulated along with kinematic relations. In fact, this theory described the mass and momentum transfer from one mixture constituent to another and it was also shown that classical Fick's law is a special case of this theory. Proceeding further, Muller [7] presented a thermodynamic version of the mixture theory for two Newtonian fluids and derived the energy equation and entropy inequality for the mixture. The development of continuum theories of mixtures from the period from 1957 to 1976 was presented in a review paper by Atkin and Craine [8] in which they derived basic equations of mixture theory including the continuity, momentum, and energy equations along with the entropy inequality. In particular, a constitutive theory for a mixture of two ideal gases was given and the results were compared with the kinetic theory of gases. On the same lines, Bowen [9] and Bedford and Drumheller [10] also furnished survey of mixture theory. Later on, Rajagopal and Tao [11] wrote an excellent book on mechanics of mixtures in which conservation laws were derived and several examples were considered and analyzed from mixture theory viewpoint. All of the above-mentioned studies were lacking the applications to biological systems in which many soft tissues behave like deformable porous media and the application of mixture theory becomes an obvious choice.

The application of mixture theory to soft biological tissues essentially started with the work of Kenyon [12–14], who discussed radial flux of fluid through a porous cylinder replicating a model of flow through arterial tissue. Following this, Jayaraman [15] studied the problem of flow through an arterial wall with constant permeability and Jain and Jayaraman [16] also investigated the same problem but considered two layers in the artery wall each with different permeabilities. Similarly, Klanchar and Tarbell [17] studied the water flow through arterial tissue by considering a linear form of the strain-dependent permeability. Apart from arterial tissue, the theory was extended further by Mow *et al.* [18–22] by considering the

articular cartilage as a deformable porous material saturated with synovial fluid. The main application, however, was the lubrication properties of synovial joints such as the knee. Due to the compression of the cartilage, the synovial fluid moves through the pores of the tissue to form a surface lubricating layer. Although, the modeling of articular cartilage is a difficult task, nevertheless, the researchers such as Mow, Lai, Holmes and many others have studied the cartilage extensively in a series of papers starting from the year 1977. The role of fluid pressurization and surface porosities on the boundary friction of articular cartilage was investigated by Ateshian *et al.* [23]. Building on the previous studies, Barry and Aldis [24–26] developed several mathematical models for flow-induced deformation of absorbing porous biological tissues. In particular, the authors used biphasic mixture theory to develop one-dimensional models to study the coupling between solid deformation and fluid flow. Similarly, other tissues that have been modeled in this manner include cornea [27], skin [28] and lung [29], etc. Another important application of mixture theory in biomechanics is the resorption phenomena in bones reconstructed with bio-resorbable materials. Lekszycki and Dell’Isola [30] presented a continuum poro-elastic mixture model where two apparent mass densities were introduced to describe the situations in which bone tissues and bio-resorbable materials coexist and interact. They focused on the final healing stage process until the bone is remodeled and eventually replaced by newly synthesized living tissue. Giorgio *et al.* [31] studied the resorption and growth in bone tissue using finite element analysis. The studies on cartilage mentioned above considered the tissue as a biphasic material, however, a big stride was made by Lai *et al.* [32, 33] in 1991 to develop a triphasic mixture theory for articular cartilage by including the two solid-fluid phases, and an ion phase, representing cation and anion of a single salt. This triphasic theory essentially combined the physico-chemical theory for ionic solutions with the biphasic mixture theory. Based on the triphasic theory, Gu *et al.* [34] investigated the negative osmotic flows through charged hydrated soft tissues and reported that the solvent would flow from high salt concentration side to the lower concentration side for a particular choice of the fixed charge density and that the negative osmosis phenomenon is due to the friction between ions and

water. Similarly, Sun *et al.* [35] investigated the mixed finite element formulation of triphasic mechano-electrochemical theory for charged hydrated biological tissues. Moreover, Myers *et al.* [36] also employed the triphasic theory of Lai to study the ion-induced deformation of soft tissues. In particular, the authors made certain simplifying assumptions to the general equations of the triphasic theory and obtained a coupled system of nonlinear partial differential equations in terms of ion concentration and tissue solid deformation in a general form which covered the Cartesian, cylindrical and spherical geometries. They predicted a lower ion concentration in a rectangular specimen of the tissue in comparison to a similar study by Myers *et al.* [37]. A spherical sample of the tissue was also considered and the numerical results indicated that the tissue may contract internally before swelling and/or swell internally before finally contracting. Finally, the authors compared the nonlinear theory with the linearized version of the problem which was obtained by considering the relative magnitudes and time variation of the terms in the governing equations. Apart from these, several other studies on the applications of triphasic theory to the soft biological tissues may be found in the references [38–40]. Moving one step ahead, Frijns *et al.* [41] proposed a quadriphasic theory including the solid, liquid, cation and anion phases of the mixture to discuss the swelling and shrinking nature of the intervertebral disc. Additionally, some more recent papers on mixture theory in combination with soft biological tissues may be found in the references [42–46].

Having described the development and applications of the mixture theory to soft biological tissues such as articular cartilage, arterial tissue, skin, lung and intervertebral disc, another important area of biology where this theory has been used is the modeling of tumor growth, cancer modelling and growth and remodeling of soft tissues. The study regarding modeling solid tumor growth using mixture theory was by Byrne and Preziosi [47]. The authors developed a two-phase model of an avascular tumor and reported the dependence of cell proliferation rate on the cellular stress and the incorporation of mass exchange between the constituents. Ambrosi and Preziosi [48] discussed the closure of mass balance models for tumor growth by introducing a suitable velocity field. The authors also presented

a critical review of the approaches used in the tumor growth modeling. Likewise, a multiphase model of the tumor and tissue growth including cell adhesion and plastic reorganization was presented by Preziosi and Vitale [49]. Their primary goal was to embed the experimental data for the detachment force of single adhesion bonds in a multicomponent model developed in the context of mixture theory. The understanding of the development and spread of cancer tumors is very important for finding cures and treatments of the disease. Thus, an effort in this regard was made by Preziosi [50] to demonstrate that how mathematical modeling and computer simulation techniques may help discover and develop an understanding of the mechanics of tumor development and growth. An insight into mixture theories for growth and remodeling was presented by Ambrosi *et al.* [51]. In particular, the authors discussed the emergence of residual stress due to growth and remodeling of soft tissues modeled as a mixture of a solid and several fluids. Ateshian and Humphrey [52] produced a review of continuum mixture models of biological growth and remodeling and considered several illustrative examples to show diverse applications of mixture theory. Moreover, the authors also identified some open problems in the area of growth and remodeling of tissues.

In the following section, a layout of the thesis presenting a brief detail of the problems considered in this thesis is presented.

1.2 Thesis Outline

The continuum mixture theory specialized to a binary mixture comprised of a solid and a fluid phase is used to examine the deformation of soft biological tissues. In particular, we develop a one-dimensional model of flow as well as ion-induced deformation of soft porous tissues. The theory used here is based on the work of Atkin and Craine [8] and Barry and Aldis [24]. Our focus in this dissertation would be to study the fluid flow through deformable porous media such as soft biological tissues with emphasis on medical and clinical applications. In the following, an outline of the chapters to be considered in this dissertation is presented.

In Chapter 2, we begin by presenting some basic definitions and concepts related to the fluid flow through deformable porous media. This is followed by an account of the basic equations of mixture theory which will be used for the development of mathematical models in later chapters. Finally, we talk about numerical methods used to solve the resulting nonlinear ordinary and partial differential equations.

In Chapter 3, we develop a mathematical model of non-Newtonian flow-induced deformation from pressurized cavities in absorbing porous biological tissue using mixture theory approach. In particular, a model with a spherical cavity embedded in a porous medium of infinite extent is used to find fluid pressure and solid displacement in the tissue as a function of radial distance and time. The tissue is assumed to be a nonlinear deformable porous material where absorption of injected fluid takes place at a rate proportional to the local fluid pressure. The steady and unsteady solutions for the fluid pressure and solid displacement as a function of non-dimensional radial distance and time are presented. In particular, effects of the power-law index and permeability parameter on fluid pressure and solid displacement profiles are illustrated graphically. This work is published in *Computer methods in biomechanics and biomedical engineering* [53] in 2017.

Application of an externally applied magnetic field to excitable tissues has been extensively used recently for biological and physiological applications with an aim to devise an accurate mechanism for the diagnosis and treatment of various diseases. Some of the biological applications of a magnetic field include drug targeting, magnetic hyperthermia, cell isolation and magnetic resonance imaging, etc. Therefore, based on the flow geometry of the previous chapter, the aim of Chapter 4 is to examine the effect of magnetohydrodynamics (MHD) on the flow-induced deformation of porous biological tissues. Here again, we use mixture theory approach to develop a mathematical model with an assumption of a linear permeability of the solid matrix. The Navier-Stokes equations coupled with the Maxwell equations of electromagnetism are used to obtain the equations in terms of fluid pressure and solid displacement. These governing equations are solved numerically to assess the influence of various pertinent parameters.

Continuing on the applications of magnetohydrodynamics, in Chapter 5, we present an MHD based mathematical model with strain-dependent nonlinear permeability to study the deformation of articular cartilage equilibrated in a sodium chloride solution. A linear biphasic mixture theory with the inclusion of ion concentration term in the solid stress equation has been employed to develop a mathematical model. In particular, a thin rectangular specimen of bovine cartilage is considered which is subjected to changes in the ionic environment under the action of a uniform applied magnetic field. The governing PDEs in terms of ion concentration, solid displacement and fluid pressure of the tissue are non-dimensionalized using appropriate dimensionless quantities and then solved analytically and numerically. Specifically, exact solutions are given for the constant permeability and numerical solutions are provided for the nonlinear permeability case to highlight the influence of magnetic and permeability parameter.

In Chapter 6, the conclusion along with a discussion for the future work is furnished. Finally, the derivation of magnetohydrodynamics (MHD) equations in the context of mixture theory are presented in the Appendix.

Chapter 2

Preliminaries

2.1 Introduction

In this chapter, some important definitions and basic concepts that will assist in understanding the fluid flow through a porous material are presented. In addition to these basic concepts, we also present fundamental equations of mixture theory including kinematic relations and balance laws. In the end, we discuss numerical methods used to solve the nonlinear equations of the problems considered in this thesis.

2.2 Porous Material

A material which contains pores or voids in it is known as the porous material. The skeletal material is usually solid and is often termed as the matrix. The pores of the material are typically filled with a liquid or a gas. Most of the materials which are encountered in science and engineering are porous in nature. Therefore, for accurate modeling, knowledge of properties of such materials is essential. A structure of a porous material is shown in Figure 2.1. In general, porous materials can be classified into two main categories i.e. rigid and deformable porous materials.

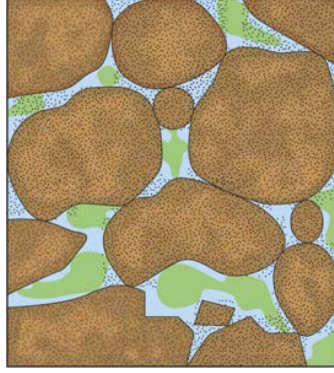


FIGURE 2.1: Basic schematic of a porous material, Lagree [54].

The materials which allow fluid to pass through them and maintain their shape and size are called rigid porous materials. Examples of such materials include wood, brick, pipe and biomedical scaffolds, etc.

Deformable porous materials are those which undergo a deformation in the form of shape or size such as sponge, artery, articular cartilage, and foam, etc. Our focus in this thesis is to understand and highlight the important features and key points related to deformable porous media by considering a few examples from biomedical field.

2.3 Porosity

The measure of empty or void spaces in a porous material is termed as porosity. Mathematically, porosity ϕ_n is a ratio of the volume of empty space to the total volume of the porous material and typically lies between 0 and 1 or equivalently expressed in percentage between 0% to 100%

$$\phi_n = \frac{V_E}{V_T}, \quad (2.1)$$

where V_E is the volume of empty space and V_T is the total volume of the porous material, including the solid as well as void components. The porosity is a dimensionless quantity as suggested by the relation (2.1). Moreover, due to a large number of empty spaces, a sponge is said to be more porous than a biological

tissue. The term porosity has been used in many branches of science such as metallurgy, manufacturing, soil mechanics and biomechanics. There are a variety of methods available with which porosity of a material can be determined, for instance, industrial CT scanning, water evaporation, gas expansion, optical and imbibition method.

2.4 Darcy's Law

During a seminal experiment on the fluid flow through a porous media, Henry Darcy, a French engineer, proposed a linear relationship between the flow rate Q^* and the pressure gradient ∇P in a single phase flow known as Darcy's law which is given by the mathematical relation

$$Q^* = -\frac{\kappa A}{\mu} \nabla P, \quad (2.2)$$

where κ is the permeability, A the specific area and μ is the viscosity of the fluid. In particular, Darcy's law is based on the result of experiments on the flow of water through beds of sand which laid down the foundation of hydrogeology, a branch of geology. The Darcy's law is valid for low Reynolds-number flow and concerns the isotropic and homogeneous porous media. This law is analogous to Fick's law in diffusion theory, Fourier's law in heat conduction and Ohm's law in electromagnetism. The Darcy's law (2.2) may be reduced to a more convenient form as

$$q = -\frac{\kappa}{\mu} \nabla P, \quad (2.3)$$

where q is the flux or discharge per unit area and negative sign here indicates the fluid flows from high pressure to low pressure. The fluid velocity in the porous material v is related to the Darcy flux q by the following relation

$$v = \frac{q}{\phi_n}, \quad (2.4)$$

where ϕ_n represents the porosity of the medium. These equations may, however, be extended easily to multi-phase flows, thus giving Darcy's law for multi-phase flows through porous media Lagree [54].

2.5 Permeability

Another important property associated with a porous material is the permeability which is defined as a measure of the ability of a porous material to allow fluid to pass through it. It is denoted by the symbols κ and measured in SI unit m^2 or more practical unit *darcy* (d). Mathematically, it may be written from equation (2.3) as

$$\kappa = \frac{-q\mu}{\nabla P}, \quad (2.5)$$

where the meaning of the negative sign is the same as described above. It is important to note that the term permeability is defined differently in different fields such as soil mechanics, electromagnetism, chemistry, and transportation. The permeability of a material depends on porosity, shape, and size of pores and the degree of their connectedness. The permeability of a material may be determined in the laboratory by application of Darcy's law for steady-state conditions or, more generally, by application of various solutions to the diffusion equation for unsteady flow conditions.

2.6 Fluid Classification

The classification of fluids is based on the concept of viscosity which is defined as the resistance of a fluid to gradual deformation either by shear stress or tensile stress. This means that a viscous fluid offers resistance to the immersed objects through them and to the motion of layers with differing velocities within them. Thus, honey is more viscous than water due to greater friction among its layers.

Formally, dynamic viscosity denoted by the symbol μ is defined to be the ratio of the shearing stress to the velocity gradient in a fluid. Mathematically, it is expressed as

$$\mu = \frac{\tau}{du/dy}, \quad (2.6)$$

where $\tau = \frac{F}{A}$ is the shear stress and $\frac{du}{dy}$ is the velocity gradient. The viscosity of a fluid is measured in $\frac{Ns}{m^2}$ in the SI system. A fluid which has zero viscosity is termed as an ideal or inviscid fluid and these fluids exist physically at very low temperatures. The ratio of the dynamic viscosity to the density of the fluid is known as the kinematic viscosity. It is denoted by the Greek symbol $\nu = \frac{\mu}{\rho}$ and measured in $\frac{m^2}{s}$ in the SI system. In general, fluids are classified into two main types, namely, Newtonian and non-Newtonian fluids. These two types of fluids cover most of the applications of industry, engineering, and biomedical sciences. Below we present brief details on both of these fluid types.

2.6.1 Newtonian Fluid

A fluid in which shear stress is directly proportional to strain rate at every point in a flow field is known as a Newtonian fluid. In other words, a Newtonian fluid obeys the empirical formula (2.6) which is essentially Newton's law of viscosity for incompressible and isotropic case. However, for the anisotropic case, the coefficient μ in equation (2.6) is replaced by a nine-element viscosity tensor μ_{ij} . Examples of Newtonian fluids include water, air, glycerol, oils, alcohol, etc.

2.6.2 Non-Newtonian Fluid

A fluid that does not obey Newton's law of viscosity described in equation (2.6) is known as a non-Newtonian fluid. The viscosity of such a fluid is not constant and depends upon the shear rate. Examples of non-Newtonian fluids include salt solutions, molten polymers, ketchup, custard, starch suspensions, honey, paints,

blood, and synovial fluid, etc. There are numerous non-Newtonian fluid models that have been developed and studied in the literature. However, one of the commonly used and related to our thesis is the power-law fluid model, for which the shear stress τ is defined as

$$\tau = K^* \frac{\partial u}{\partial y} \left| \frac{\partial u}{\partial y} \right|^{n-1}, \quad (2.7)$$

where K^* is the flow consistency index, $\frac{\partial u}{\partial y}$ the shear rate and n the power-law index. Note that the relation (2.7) is derived from the stress tensor $\tau_{ij} = 2K^*(2D_{kl}D_{kl})^{\frac{n-1}{2}} \cdot D_{ij}$ for power-law fluid [55] where $D_{ij} = \frac{1}{2}(\frac{\partial u_i}{\partial x_j} + \frac{\partial u_j}{\partial x_i})$ represents the stretching tensor. Moreover, the quantity $\mu_{\text{eff}} = K^* \left| \frac{\partial u}{\partial y} \right|^{n-1}$ is termed as an apparent or effective viscosity for the power-law fluid. It is important to note that power-law fluid is further classified as shear-thinning and shear-thickening fluid depending upon the power-law index n in equation (2.7) is less or greater than unity, whereas $n = 1$, yields the Newtonian fluid case.

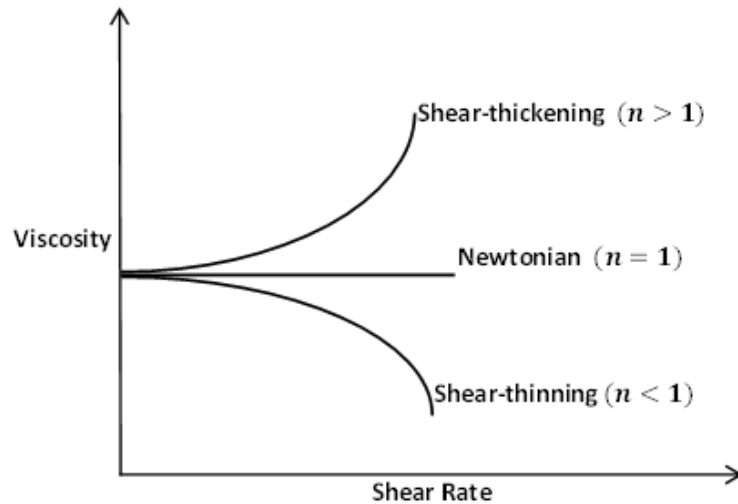


FIGURE 2.2: Relation between shear rate and viscosity for a power-law fluid.

As shown in Figure 2.2, in shear-thinning or pseudoplastic fluids, viscosity decreases by increasing the shear rate such as polymer solutions, paints, and bio-fluids whereas in shear-thickening or dilatant fluids, viscosity increases with the

shear rate, for example, the cornstarch solution, etc. The other important feature that is presented in this thesis is to combine magnetohydrodynamics with mixture theory modeling.

2.7 Magnetohydrodynamics

Magnetohydrodynamics (MHD) is a branch of physics which is related to the dynamics of the magnetic field in electrically conducting fluids, for instance, plasmas, liquid metals, electrolytes and salt water. The credit of pioneering this field goes to a Swedish physicist Hannes Alfvén in 1942. The main idea of MHD is that magnetic fields can induce currents in a moving conductive fluid which are capable of altering the magnetic field itself. The Navier-Stokes equations coupled with Maxwell equations are used to describe the dynamics in an MHD system, whose details are presented in the Appendix. Although, MHD was originally applied to the problems of astrophysics and geophysics but its applications have now encompassed many other fields of science such as magnetochemistry, magnetobiology and bioelectromagnetism, etc. The externally applied magnetic field has significant effects on physiological systems. It has been established that applied magnetic field stimulates the functions of biological tissues and also regenerates the tissues in the body [56]. Moreover, a magnetic field is successfully used recently for the diagnostic and treatment of many hazardous diseases such as cancer and tumors in the body. In addition to these, our body contains magnetic fluids, which may assist in cell isolation and drug targeting for clinical purposes under the suitably designed magnetic field.

2.8 Biological Tissue

A biological tissue is defined as a group of cells in an organism which has identical structure and capable of performing the same function. The biological tissues in animals are classified into four different types: connective, epithelial, muscle and

nervous as shown in Figure 2.3. The group of tissues makes up organs in the animal body such as the heart, brain, and lungs, etc. On the other hand, soft tissues are those which connect, support and surround other organs of the body such as ligaments, nerves, fascia, tendons, fibrous tissues and synovial membranes. Soft tissues are composed of collagen, elastin and the ground substance and exhibit viscoelastic properties which make them amenable to the mathematical and physical analysis. Understanding the behavior of biological tissues under different physical situations is important from medical as well as clinical point of view.

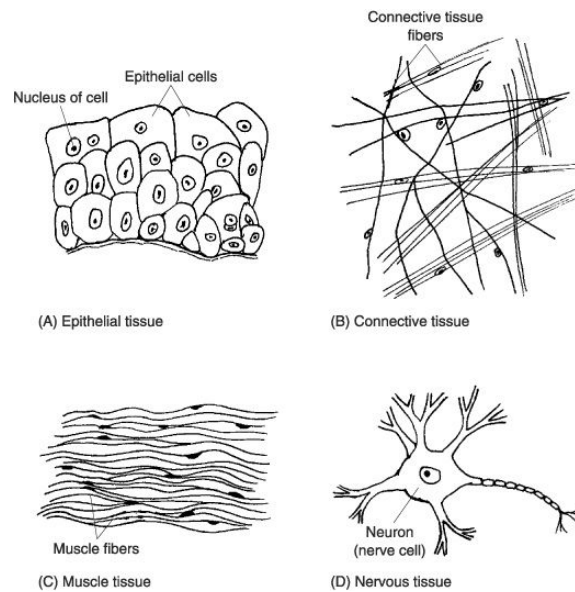


FIGURE 2.3: Types of tissue [57].

As noted by Humphrey [1] and mentioned in the introductory chapter, there are several theoretical frameworks available in the literature for modeling biological tissues. Among these theories, one of well accepted and widely used is the mixture theory, which we utilize in this study to investigate the solid-fluid interaction in porous tissues. In the following, we briefly present some basics of continuum mixture theory.

2.9 Mixture Theory: Kinematics and Balance Laws

Most of the materials whether natural or man-made are mixtures as they consist of more than one constituents. But the need for continuum mixture theory arises whenever there is a relative motion between the constituents of the mixture or the constituents exchange mass. Biological systems tend to exhibit both phenomena, thus paving the way for enormous potential of mixture theory for biomechanics. The basic tenets of mixture theory are [58] (i) at each instant of time, every point of the spatial domain of the mixture is simultaneously occupied by all the components of the mixture and (ii) with suitable choices of variables, the mixture as a whole obeys the standard balance laws of classical continuum mechanics. In the following, we present kinematics and balance laws for a mixture of N identifiable components.

Consider a mixture of N immiscible constituents which are supposed to occupy each material point in space at the same time. The motion of the components of the mixture is described by smooth functions

$$\mathbf{x} = \chi^\eta(\mathbf{X}^\eta, t), \quad (2.8)$$

where $\eta = 1, 2, 3, \dots, N$ and \mathbf{X}^η denote the position of the particle in the reference configuration. The inverse of the function χ^η can be expressed as

$$\mathbf{X}^\eta = \zeta^\eta(\mathbf{x}, t). \quad (2.9)$$

The mass density of the mixture, ρ , may be defined as

$$\rho = \sum_{\eta=1}^N \rho^\eta, \quad (2.10)$$

where ρ^η is the mass density of the η^{th} constituent of the mixture. The volume fraction ϕ^η of the η^{th} constituent of the mixture is defined as

$$\phi^\eta = \frac{\rho^\eta}{\rho_R^\eta}, \quad (2.11)$$

where ρ_R^η is the density for the η^{th} constituent in a homogeneous state. For a saturated mixture, the volume fractions must satisfy the following constraint

$$\sum_{\eta=1}^N \phi^\eta = 1. \quad (2.12)$$

The velocity \mathbf{v}^η and deformation gradient \mathbf{F}^η of the particle \mathbf{X}^η may be defined as

$$\mathbf{v}^\eta = \frac{\partial}{\partial t} \chi^\eta(\mathbf{X}^\eta, t), \quad \mathbf{F}^\eta = \nabla \chi^\eta(\mathbf{X}^\eta, t), \quad (2.13)$$

where ∇ represents the gradient operator with respect to spatial position. The mean velocity \mathbf{v} and diffusion velocity \mathbf{u}^η of the mixture can be written as

$$\mathbf{v} = \frac{1}{\rho} \sum_{\eta=1}^N \rho^\eta \mathbf{v}^\eta, \quad \mathbf{u}^\eta = \mathbf{v}^\eta - \mathbf{v}. \quad (2.14)$$

The material time derivative $\frac{D^\eta}{Dt}$ of the η^{th} constituent of the mixture is defined as [8, 59]

$$\frac{D^\eta(\cdot)}{Dt} = \frac{\partial(\cdot)}{\partial t} + \{(\mathbf{v}^\eta \cdot \nabla)(\cdot)\}. \quad (2.15)$$

Similarly, the material time derivative $\frac{D}{Dt}$ for the mixture as a whole is written as

$$\frac{D(\cdot)}{Dt} = \frac{\partial(\cdot)}{\partial t} + \{(\mathbf{v} \cdot \nabla)(\cdot)\}. \quad (2.16)$$

We now turn our attention to the formulation of balance laws for the mixture. In Eulerian formulation, the conservation of mass and linear momentum for the η^{th} component of the mixture is given by Atkin and Craine [8]

$$\frac{\partial \rho^\eta}{\partial t} + \nabla \cdot (\rho^\eta \mathbf{v}^\eta) = \rho^\eta \Phi^\eta, \quad (2.17)$$

$$\frac{\partial}{\partial t}(\rho^n \mathbf{v}^n) + \nabla \cdot (\rho^n \mathbf{v}^n \otimes \mathbf{v}^n) = \nabla \cdot \mathbf{T}^n + \rho^n \mathbf{b}^n + \boldsymbol{\pi}^n + \rho^n \Phi^n \mathbf{v}^n, \quad (2.18)$$

where $\rho^n \Phi^n$ is the mass supply rate, \mathbf{T}^n the stress tensor, $\rho^n \mathbf{b}^n$ the body force and $\boldsymbol{\pi}^n$ the internal interaction force of the η^{th} constituent of the mixture. Note that for a binary mixture of solid and fluid (i.e. $\eta = 1, 2$), the conservation laws (2.17)- (2.18) will be used under certain assumptions in the following chapters for the development of mathematical models. The balance of mass (2.17) and linear momentum (2.18) upon simplification take the following form [59]

$$\frac{\partial \rho}{\partial t} + \nabla \cdot (\rho \mathbf{v}) = 0, \quad (2.19)$$

$$\rho \frac{D\mathbf{v}}{Dt} = \nabla \cdot \mathbf{T} + \rho \mathbf{b}, \quad (2.20)$$

where the assumptions $\sum_{\eta=1}^N \rho^n \Phi^n = 0$ and $\sum_{\eta=1}^N (\rho^n \Phi^n \mathbf{v}^n + \boldsymbol{\pi}^n) = 0$ have been used. It is important to note that we do not consider the temperature and rotational effects here, therefore, for brevity, only the conservation of mass and linear momentum for the mixture are presented above. However, conservation of angular momentum and energy along with entropy inequality for the mixture may also be described in a similar manner [8].

2.10 Numerical Method and Matlab Solvers

In this section, we present numerical methods which will be used to solve the resulting nonlinear ordinary and partial differential equations in the chapters to follow. In particular, we first present the method of lines along with an illustrating example. This is followed by a discussion on Matlab solvers *bvp4c* and *pdepe*.

2.10.1 Method of Lines

The method of lines (MOL) is a general numerical procedure used to solve the time-dependent partial differential equations, usually one-dimensional parabolic or elliptic PDEs [60, 61]. MOL is a semi-analytical technique in which the spatial derivatives are discretized leaving the time variable continuous. This leads to a system of coupled ordinary differential equations (ODEs) which can then be solved using numerical methods for initial value problems. The salient features of the MOL which justify its use include: computational efficiency, numerical stability, reduced programming effort and reduced computational time. In order to illustrate this method, we consider one-dimensional heat equation and compare the result with the exact solution. Consider the problem

$$\frac{\partial u}{\partial t} = \frac{\partial^2 u}{\partial x^2}, \quad 0 < x < 1, \quad t > 0, \quad (2.21)$$

subject to the following conditions

$$u(x, 0) = 1, \quad u(0, t) = 0, \quad u(1, t) = 0, \quad (2.22)$$

which admits the closed form solution

$$u(x, t) = \frac{4}{\pi} \sum_{k=0}^{\infty} \frac{1}{(2k+1)} \sin \{(2k+1)\pi x\} e^{-(2k+1)^2 \pi^2 t}. \quad (2.23)$$

As required by the MOL, we discretize the spatial derivative appearing on the right hand side of equation (2.21) by using central finite difference scheme accurate up to second order and write

$$\frac{du_i}{dt} = \frac{u_{i+1} - 2u_i + u_{i-1}}{h^2}, \quad i = 1, 2, 3, \dots, N, \quad (2.24)$$

where $u_0 = 0$ and $u_{N+1} = 0$ is obtained from the left and right boundary condition respectively, and

$$u_i = u(x_i, t), \quad h = \frac{1}{N}, \quad x_i = ih. \quad (2.25)$$

The initial conditions at each node may be expressed from the first equation in (2.22) as

$$u(x_i, 0) = 1. \quad (2.26)$$

We thus have a system of N ODEs (2.24) and the corresponding initial conditions outlined in equation (2.26), which may now be solved using well established and efficient Matlab's ODE solvers such as *ode23s*.

In Figure 2.4, we present a graphical comparison between the exact and numerical (MOL) solution of the heat equation (2.21) at $t = 0.95$. An excellent agreement between the two solutions can be noticed which validates the proposed numerical scheme. Also, note that choice of time in this graph is random, however, different values of the time may also be considered.

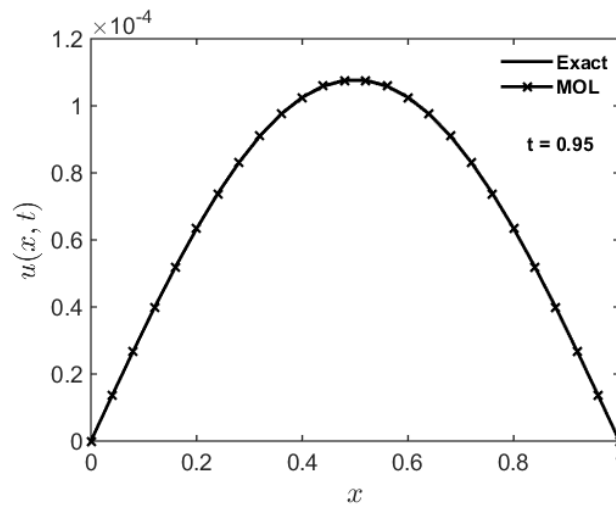


FIGURE 2.4: A comparison between the exact and MOL solution of the heat equation (2.21).

In addition to a graphical comparison, we also present a comparison in the form of table between the two solutions by varying time and number of spatial nodes. The maximum absolute error between the exact and numerical solution in Table 2.1 for different number of spatial nodes N and time t justifies that MOL scheme meets the required order of accuracy.

Error = max (Exact - MOL)				
Number of Nodes	Time			
N	$t = 0.1$	$t = 0.5$	$t = 0.75$	$t = 0.80$
25	1.1918×10^{-4}	4.1465×10^{-5}	3.8468×10^{-6}	1.9989×10^{-6}
100	1.1849×10^{-4}	1.1501×10^{-6}	1.8441×10^{-6}	1.6577×10^{-6}
300	1.1796×10^{-4}	9.6002×10^{-7}	1.4369×10^{-6}	1.3606×10^{-6}

TABLE 2.1: Maximum absolute error between the exact and MOL solution of heat equation (2.21) for different times and spatial nodes.

2.10.2 `bvp4c`

The predefined Matlab function `bvp4c` is a finite difference code that utilizes a collocation method to solve a two-point nonlinear boundary value problem in a finite domain by dividing the interval of integration into sub-intervals and solving a system of algebraic equations obtained from the collocation conditions Esfandari [62]. Additionally, `bvp4c` computes the error of approximate solution on each subinterval. If a tolerance criterion is not met, the solver modifies the mesh and repeats the procedure. In order to begin a numerical experiment, `bvp4c` requires initial points of the mesh along with initial guess of the solution at the mesh points and of the unknown parameters. Thus, in summary, `bvp4c` requires three pieces of information: the equation to be solved, its relevant boundary conditions, and initial guess for the solution and the parameters.

2.10.3 `pdepe`

The predefined function `pdepe`, which stands for parabolic-elliptic partial differential equations, is a Matlab built-in function used to numerically solve initial-boundary value problems for a class of parabolic and elliptic PDEs usually in one space dimension [63]. The function `pdepe` is based on method of lines technique that converts the PDEs into a system of coupled ODEs by discretizing the space derivatives using finite differences accurate up to second order and leaving the

time variable continuous. Then the resulting ODEs are integrated using a stiff ODE solver *ode15s* to obtain approximate solutions at various times. However, for complex geometries and nonclassical boundary conditions, one has to develop a different MOL code which may be validated by *pdepe* in the special case.

Chapter 3

Non-Newtonian Flow-Induced Deformation From Pressurized Cavities in Absorbing Porous Tissues

3.1 Introduction

In this chapter, a mathematical model of non-Newtonian flow-induced deformation from pressurized cavities in the absorbing porous biological tissues has been developed and discussed. In particular, the tissue is modeled as a nonlinear deformable porous material where the injected power-law fluid is absorbed by the tissue at a rate proportional to the local fluid pressure. A spherical cavity embedded in an infinite porous medium is used to find the fluid pressure and solid displacement in the tissue as a function of radial distance and time. The governing nonlinear equations are solved numerically to highlight the effects of various emerging parameters. In particular, it is noted that the shear-thickening fluids exhibit less fluid pressure and induce small solid deformation in comparison to the

shear-thinning fluids. Moreover, fluid pressure and solid displacement are increasing functions of the permeability parameter as well as the absorption parameter. A graphical comparison to the previously available literature for the Newtonian fluid case is also presented. The current chapter is based on the work of Siddique and Anderson [64] which was the only available power-law model in combination with the mixture theory for the capillary rise of power-law fluid into a deformable porous material.

In Section 3.2, the mathematical formulation of the problem using the modern mixture theory approach has been presented. This is followed by an account of the boundary conditions between the fluid and the porous material in Section 3.3. The results along with discussion have been presented in Section 3.4 followed by conclusion in Section 3.5.

3.2 Mathematical Formulation

In order to develop the mathematical model, we consider a spherical cavity embedded in a porous biological tissue of infinite extent as shown in Figure 3.1. The tissue is modeled as a nonlinear deformable porous material consisting of a mixture of a solid and a fluid phase. The problem is modeled using mixture theory approach. The main underlying idea of mixture theory is that each constituent of the mixture is continuous and occupies every point in the space at each instant of time.

We assume that the fluid is a non-Newtonian viscous fluid which follows power-law model and further suppose that the elastic solid matrix is homogeneous, isotropic and body as well as osmotic forces are neglected. It is also assumed that the shear stresses are negligible on account of one dimensional radial flow and the constituents of the mixture are intrinsically incompressible and that the elastic properties of the medium are linear.

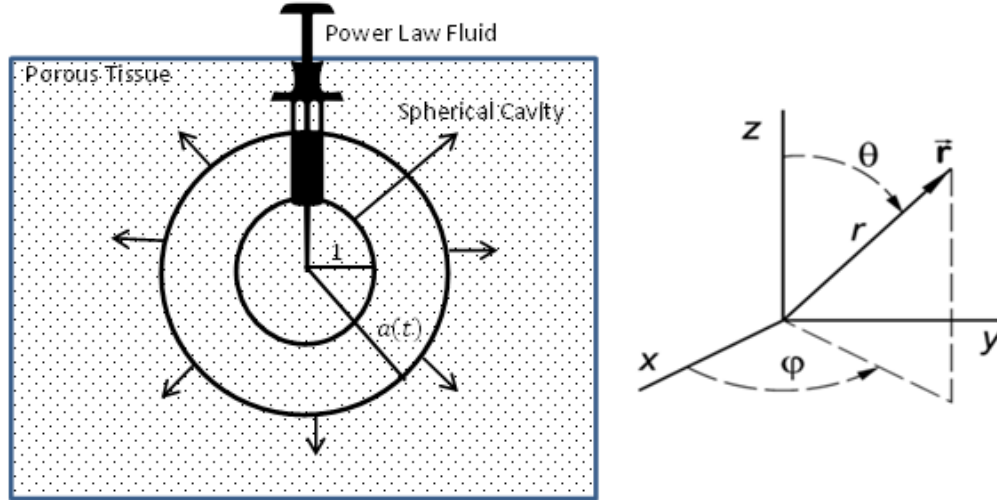


FIGURE 3.1: Diagram and coordinate system for power-law fluid flow from an injection site in a porous medium. Growth of the cavity from radius 1 to $a(t)$ is shown.

The apparent densities of individual constituents of the mixture are written as

$$\rho^\eta = \lim_{dV \rightarrow 0} \frac{dm^\eta}{dV}, \quad (3.1)$$

where $\eta = s, \ell$ represents either the solid or fluid phase, dm^η is the mass of the η phase in the small volume dV . The true density ρ_T^η and relative porosity ϕ^η of the η phase of the mixture are defined as

$$\rho_T^\eta = \lim_{dV^\eta \rightarrow 0} \frac{dm^\eta}{dV^\eta}, \quad (3.2)$$

$$\phi^\eta = \lim_{dV \rightarrow 0} \frac{dV^\eta}{dV}, \quad (3.3)$$

where dV^η is the small volume of the η phase. Using equations (3.2) and (3.3) into (3.1), we get a relation between density and porosity as

$$\rho^\eta = \phi^\eta \rho_T^\eta. \quad (3.4)$$

The relations for densities and porosities of the solid and fluid phase can be written as Barry and Aldis [24]

$$\rho^s + \rho^\ell = \rho, \quad (3.5)$$

$$\phi^s + \phi^\ell = 1. \quad (3.6)$$

The balance of mass for the solid and fluid phase is written respectively as Barry and Aldis [24]

$$\frac{\partial \rho^s}{\partial t} + \nabla \cdot (\rho^s \mathbf{v}^s) = 0, \quad (3.7)$$

$$\frac{\partial \rho^\ell}{\partial t} + \nabla \cdot (\rho^\ell \mathbf{v}^\ell) = -\beta p, \quad (3.8)$$

where \mathbf{v}^s and \mathbf{v}^ℓ are velocities of the solid and fluid phase, respectively, β is the proportionality constant which depends upon the concentration of capillaries and lymphatics in the biological tissue and permeability of their walls and p is the fluid pressure. Note that the term appearing on right hand side of equation (3.8) is due to the loss of fluid mass at a rate proportional to the fluid pressure while it passes through capillaries and lymphatics. Invoking the relation (3.4) into the continuity equations (3.7) and (3.8), we obtain

$$\frac{\partial \phi^s}{\partial t} + \nabla \cdot (\phi^s \mathbf{v}^s) = 0, \quad (3.9)$$

$$\frac{\partial \phi^\ell}{\partial t} + \nabla \cdot (\phi^\ell \mathbf{v}^\ell) = -\frac{\beta p}{\rho_T^\ell}. \quad (3.10)$$

Adding equations (3.9) and (3.10) and making use of the relation (3.6) leads to

$$\nabla \cdot \mathbf{v} = -\frac{\beta}{\rho_T^\ell} p, \quad (3.11)$$

where

$$\mathbf{v} = \mathbf{v}^s \phi^s + \mathbf{v}^\ell \phi^\ell, \quad (3.12)$$

is defined to be the macroscopic or composite velocity of the mixture. The conservation of linear momentum for the η^{th} component of the mixture as described in the previous chapter is rewritten here as

$$\rho^\eta \left(\frac{\partial \mathbf{v}^\eta}{\partial t} + (\mathbf{v}^\eta \cdot \nabla) \mathbf{v}^\eta \right) = \nabla \cdot \mathbf{T}^\eta + \rho^\eta \mathbf{b}^\eta + \boldsymbol{\pi}^\eta, \quad (3.13)$$

where \mathbf{T}^η is the stress tensor and \mathbf{b}^η the net body force of the η phase whereas $\boldsymbol{\pi}^\eta$ represents the internal frictional interaction force between the mixture constituents. The inertial terms appearing on the left hand side of equation (3.13) are taken into account for the derivation of governing equations by Barry and Aldis [65] and proven to be negligible for a particular choice of time scale but our reason for neglecting these terms is due to small velocities and deformation rates that reduces the momentum equation (3.13) to the following form

$$\nabla \cdot \mathbf{T}^\eta + \boldsymbol{\pi}^\eta = \mathbf{0}, \quad (3.14)$$

where body forces are neglected and Newton's third law for internal frictional forces means that $\boldsymbol{\pi}^s + \boldsymbol{\pi}^\ell = \mathbf{0}$. The stress tensor \mathbf{T}^η may be defined as [24]

$$\mathbf{T}^\eta = -\phi^\eta p \mathbf{I} + \boldsymbol{\sigma}^\eta, \quad (3.15)$$

where $\boldsymbol{\sigma}^\eta$ represents either the solid or fluid stress and \mathbf{I} is the identity tensor. In this chapter, we neglect the viscous stress $\boldsymbol{\sigma}^\ell$ on account of one-dimensional radial flow and assume that $\boldsymbol{\sigma}^s = \boldsymbol{\sigma}$ for the rest of the derivation. It is worth noting that in usual non-Newtonian fluid modeling, the rheological effects enter into the governing equations from the viscous stress $\boldsymbol{\sigma}^\ell$ whereas in the present mathematical model under above-mentioned assumptions, the rheological effects enter through the drag forces $\boldsymbol{\pi}^\eta$. The drag force for the power-law fluid in a deformable porous medium is defined as [64]

$$-\boldsymbol{\pi}^s = \boldsymbol{\pi}^\ell = K (\mathbf{v}^s - \mathbf{v}^\ell) |\mathbf{v}^s - \mathbf{v}^\ell|^{n-1} - p \nabla \phi^s, \quad (3.16)$$

where K is the drag coefficient of relative motion and n is the power-law index

with $n < 1$ for shear-thinning, and $n > 1$ for shear-thickening fluids. Setting $n = 1$, in this equation, yields the relation for the Newtonian fluid case [24] and taking $\mathbf{v}^s = \mathbf{0}$ and $\phi^s = \text{constant}$ gives rigid non-Newtonian fluid case. Using equation (3.15) into (3.14) and taking into account the assumptions $\boldsymbol{\sigma}^s = \boldsymbol{\sigma}$ and $\boldsymbol{\sigma}^\ell = \mathbf{0}$, yields

$$\nabla \cdot (-\phi^s p \mathbf{I} + \boldsymbol{\sigma}) + \boldsymbol{\pi}^s = \mathbf{0}, \quad (3.17)$$

$$\nabla \cdot (-\phi^\ell p \mathbf{I}) + \boldsymbol{\pi}^\ell = \mathbf{0}. \quad (3.18)$$

Adding equations (3.17) and (3.18) and making use of the relations $\phi^s + \phi^\ell = 1$ and $\boldsymbol{\pi}^s + \boldsymbol{\pi}^\ell = \mathbf{0}$ allows us to write

$$\nabla \cdot \boldsymbol{\sigma} = \nabla p. \quad (3.19)$$

Substituting the relations for $\boldsymbol{\pi}^s$ and $\boldsymbol{\pi}^\ell$ from equation (3.16) into (3.14) and taking into account equation (3.6), we have

$$\nabla \cdot \boldsymbol{\sigma} = K |\mathbf{v}^s - \mathbf{v}^\ell|^{n-1} (\mathbf{v}^s - \mathbf{v}^\ell) + \phi^s \nabla p, \quad (3.20)$$

$$\mathbf{0} = -K |\mathbf{v}^s - \mathbf{v}^\ell|^{n-1} (\mathbf{v}^s - \mathbf{v}^\ell) + \phi^\ell \nabla p. \quad (3.21)$$

Eliminating the pressure p from these equations and writing the resulting equation in terms of \mathbf{u} and \mathbf{v} , gives

$$\nabla \cdot \boldsymbol{\sigma} = \frac{1}{\kappa} \left(\frac{\partial \mathbf{u}}{\partial t} - \mathbf{v} \right)^n, \quad (3.22)$$

where

$$\kappa = \frac{(\phi^\ell)^{n+1}}{K}, \quad (3.23)$$

is the permeability of the medium which reduces to the corresponding relation in [24] for power-law index $n = 1$. Here, \mathbf{u} denotes displacement of the solid and $\mathbf{v}^s = \frac{\partial \mathbf{u}}{\partial t}$. Equation (3.22) can be explained physically by taking into account the Darcy's law and considering the solid stress as being governed by the standard

equilibrium equation of the theory of linear elasticity. As suggested by the relation (3.23), the permeability κ of the porous medium decreases as a consequence of solid compression. Following Barry and Aldis [24], we assume that $\kappa = \kappa(\phi)$, where ϕ denotes the change in porosity (or dilatation) of the medium. Many authors [17, 18, 24, 64, 66, 67] have considered different forms of this functional relation to account for the motion of fluid through various porous media.

In order to develop the governing equations of motion, we assume that solid deformations are very small so that by symmetry only the radial components of displacement and velocity are nonzero and that the permeability function κ depends only on the porosity of the medium, ϕ . The solid stress components are defined as

$$\sigma_{rr} = (\lambda + 2\mu) \frac{\partial u}{\partial r} + 2\lambda \frac{u}{r}, \quad (3.24)$$

$$\sigma_{\theta\theta} = (\lambda + 2\mu) \frac{u}{r} + \lambda \frac{\partial u}{\partial r} + \lambda \frac{u}{r} = \sigma_{\phi\phi}, \quad (3.25)$$

where λ and μ are Lamé stress constants. All other stress components are assumed to be zero. The divergence of the stress in the radial direction is given by

$$(\nabla \cdot \boldsymbol{\sigma})_r = \frac{\partial \sigma_{rr}}{\partial r} + 2 \frac{\sigma_{rr} - \sigma_{\theta\theta}}{r}. \quad (3.26)$$

Substitution of the relations (3.24) and (3.25) into equation (3.26) results into

$$(\nabla \cdot \boldsymbol{\sigma})_r = (\lambda + 2\mu) \left[\frac{\partial^2 u}{\partial r^2} + \frac{2}{r} \frac{\partial u}{\partial r} - \frac{2}{r} u \right]. \quad (3.27)$$

This may be written in a compact form as

$$(\nabla \cdot \boldsymbol{\sigma})_r = H_a \frac{\partial \phi}{\partial r}, \quad (3.28)$$

where $H_a = \lambda + 2\mu$ is the aggregate modulus of the solid matrix and the porosity ϕ in terms of displacement u is given by

$$\phi = \frac{1}{r^2} \frac{\partial}{\partial r} (r^2 u). \quad (3.29)$$

Taking into account equations (3.19) and (3.28), the governing equation (3.22) can be written in the radial direction as

$$\frac{\partial p}{\partial r} = H_a \frac{\partial \phi}{\partial r} = \frac{1}{\kappa(\phi)} \left(\frac{\partial u}{\partial t} - v_r \right)^n, \quad (3.30)$$

which on equating and integrating the first two expressions leads to

$$p(r, t) = H_a \phi(r, t), \quad (3.31)$$

where both p and ϕ tend to zero as $r \rightarrow \infty$. From equations (3.30) and (3.31), we can get a relation for v_r as

$$v_r(r, t) = \frac{\partial u}{\partial t} - \left(\kappa \left(\frac{p}{H_a} \right) \frac{\partial p}{\partial r} \right)^{\frac{1}{n}}. \quad (3.32)$$

Following Barry and Aldis [24], we consider the permeability function κ as

$$\kappa(p) = \kappa(H_a \phi) = e^{mp}, \quad (3.33)$$

where m is a material constant. Note that $m = 0$ corresponds to constant permeability case whereas $m > 0$ represents nonlinear permeability case. Plugging the expression (3.32) into the continuity equation (3.11) and using the definition of divergence for spherical coordinates, yields

$$\frac{1}{r^2} \frac{\partial}{\partial r} \left(r^2 \frac{\partial u}{\partial t} \right) - \frac{1}{r^2} \frac{\partial}{\partial r} \left\{ r^2 \left(\kappa \left(\frac{p}{H_a} \right) \frac{\partial p}{\partial r} \right)^{\frac{1}{n}} \right\} = -\frac{\beta}{\rho_T^{\ell}} p. \quad (3.34)$$

The above equation is non-dimensionalized using the following dimensionless quantities

$$\bar{t} = \frac{t}{t_0}, \quad \bar{r} = \frac{r}{r_0}, \quad \bar{p} = \frac{p}{p_0}, \quad \bar{u} = \frac{u}{u_0}, \quad \bar{\kappa} = \frac{\kappa}{\kappa_0}, \quad (3.35)$$

where t_0, r_0, p_0, u_0 and κ_0 are typical time, radius, pressure, deformation and undeformed permeability scales, respectively. After introducing these choices and using equations (3.29) and (3.31), equation (3.34) on dropping the bars assumes

the following form

$$\frac{\partial p}{\partial t} = \frac{\alpha}{r^2} \frac{\partial}{\partial r} \left\{ r^2 \left(\kappa(p\delta) \frac{\partial p}{\partial r} \right)^{\frac{1}{n}} \right\} - \omega p, \quad (3.36)$$

where

$$\alpha = \frac{H_a t_0 \kappa_0^n p_0^{\frac{1}{n} \frac{1-n}{n}}}{r_0^{\frac{n+1}{n}}}, \quad \delta = \frac{p_0}{H_a}, \quad \omega = \frac{\beta H_a t_0}{\rho_T^\ell}. \quad (3.37)$$

Note that values of various parameters involved in this equation may differ considerably among biological tissues [24]. The equation (3.36) is required governing equation in terms of fluid pressure p as a function of radial distance r and time t which is related to the porosity ϕ via equation (3.31). This equation is parabolic in nature and highly nonlinear due to the presence of power-law index n , which evidently makes it difficult to solve analytically. Moreover, it is worth mentioning that setting power-law index $n = 1$, recovers the Newtonian fluid case [24]. We choose

$$t_0 = \frac{r_0^{\frac{n+1}{n}}}{H_a \kappa_0^n p_0^{\frac{1}{n} \frac{1-n}{n}}}, \quad (3.38)$$

so that $\alpha = 1$, which then allows us to write ω in equation (3.37) as

$$\omega = \frac{\beta r_0^{\frac{n+1}{n}}}{\rho_T^\ell \kappa_0^n p_0^{\frac{1}{n} \frac{1-n}{n}}}. \quad (3.39)$$

This is to remark here that using simple dimensional analysis, right hand side of equation (3.38) can be shown to have the dimensions of length over power-law velocity. Moreover, the diffusion time scale for the Newtonian fluid case can be recovered by setting $n = 1$ in equation (3.38).

3.3 Initial and Boundary Conditions

In this section, we outline the initial and boundary conditions required to solve the governing equation for a spherical cavity embedded in an infinite porous medium presented geometrically in the previous section. It is important to note that Hou *et al.* [68] established the general boundary conditions at the interface between a binary mixture (articular cartilage) and a viscous fluid (synovial fluid) which may be Newtonian or non-Newtonian. They used the biphasic mixture theory to develop a set of boundary conditions using the conservation laws of mass, momentum and energy. The proposed boundary conditions were validated by imposing the Couette and Poiseuille flow conditions for a Newtonian viscous fluid on a porous-permeable biphasic material and the Taylor slip condition was derived. The boundary conditions for the fluid pressure and solid displacement of the porous tissue are given by [24]

$$p(r, 0) = f(r), \quad p(a, t) = g(t), \quad p(r, t) \rightarrow 0 \quad \text{as } r \rightarrow \infty, \quad (3.40)$$

and

$$\left[\frac{\partial u}{\partial r} + 2\bar{\lambda} \frac{u}{r} \right]_{r=a} = 0, \quad u(r, t) \rightarrow 0 \quad \text{as } r \rightarrow \infty, \quad (3.41)$$

where $f(r)$ and $g(t)$ are some specified functions and $\bar{\lambda} = \frac{\lambda}{\lambda+2\mu}$. Note that the given displacement boundary condition for infinitesimal deformation was derived from general boundary condition between a fluid and a porous material [68]. A similar version of boundary condition for radial flow through cylindrical shells was considered by [13, 17]. Although, we choose to use the same boundary conditions [24], however, modeling with non-Newtonian fluid models presents many interesting features both physically and numerically. Keeping in view the exponentially decaying behavior of fluid pressure $p(r, t)$ for the Newtonian fluid case, we consider $f(r) = e^{-r}$. The inner radius of the cavity $a(t)$, appearing in the

boundary conditions, is written as

$$a(t) = u(a(t), t) + a(0). \quad (3.42)$$

Note that this displacement condition, which defines a moving domain problem, is generally a nonlinear implicit equation which may be solved numerically. This moving boundary value problem presents many complexities in numerical computations. Thus, in order to simplify the system, we follow Barry and Aldis [24] and assume that the initial position of the boundary $a(0)$ is close to the final position $a(t)$, which allows us to write

$$a(t) = u(a(0), t) + a(0). \quad (3.43)$$

The boundary conditions are applied at $a(0)$ rather than $a(t)$ and this approximation is valid for infinitesimal solid displacements. Moreover, for numerical simulation, we have chosen the cavity radius $a(t) = 1$, which assists in comparing the results with Barry and Aldis [24]. However, different values of the cavity radius may also be considered.

In order to describe the motion of the solid matrix, we seek a relation that shows a connection between the solid displacement $u(r, t)$ and the fluid pressure $p(r, t)$. For this, we combine equations (3.29), (3.31) and (3.35) to write

$$p(r, t) = \frac{1}{\gamma r^2} \frac{\partial}{\partial r} (r^2 u), \quad (3.44)$$

where $\gamma = \frac{p_0 r_0}{H_a u_0}$ is a dimensionless parameter. Equation (3.44) on integration with respect to r and application of displacement boundary condition (3.41), yields

$$u(r, t) = \frac{\gamma}{r^2} \left\{ \int_{a(t)}^r s^2 p(s, t) ds + \frac{a^3(t)g(t)}{2(1-\bar{\lambda})} \right\}, \quad (3.45)$$

which on substituting $r = a(t)$ gives

$$a(t) = a(0) \left[1 - \frac{\gamma g(t)}{2(1-\bar{\lambda})} \right]^{-1}. \quad (3.46)$$

The governing equations (3.36) and (3.45) along with initial and boundary conditions suggest that exact solutions are not possible even for the simple case of constant permeability and we solve them numerically. The steady-state solutions are computed using *bvp4c* solver whereas for unsteady version of these governing equations, we use *pdepe* solver that were discussed in Chapter 2. The equation for the solid displacement of the tissue is solved using the trapezoidal rule of numerical integration for the constant as well as non-linear permeability case. The justification of our numerical solutions is presented in Figure 3.5 later in the discussion section.

3.4 Results and Discussion

In this section, we outline the outcomes of numerical computations for pressure and displacement of the porous tissue for various values of power-law index n , permeability parameter m and the absorption parameter $\xi(= \frac{\omega}{\alpha})$.

Figure 3.2 shows fluid pressure $p(r, t)$ as a function of time for constant permeability ($m = 0$). It is important to note in this figure that we used three different values of the power-law index n along with two different pressure functions $g(t)$ for radial distance to be $r = 1.1$. The two pressure functions that are being used here are $g(t) = e^{-2t}$ and $g(t) = t^{\frac{1}{2}}e^{-2t}$. When $g(t) = e^{-2t}$, the power-law fluid pressure falls exponentially shown by solid lines whereas for $g(t) = t^{\frac{1}{2}}e^{-2t}$, we observe an initial increase in power-law fluid pressure which eventually decreases exponentially after reaching to its local maximum value shown by dashed lines. Similar dynamics was observed by Barry and Aldis [24] with the exception of shear-thinning and shear-thickening property of the power-law fluid which is an important key point of the current study. Moreover, for both pressure functions, fluid pressure drops slowly for shear-thinning fluids as compared to shear-thickening fluids.

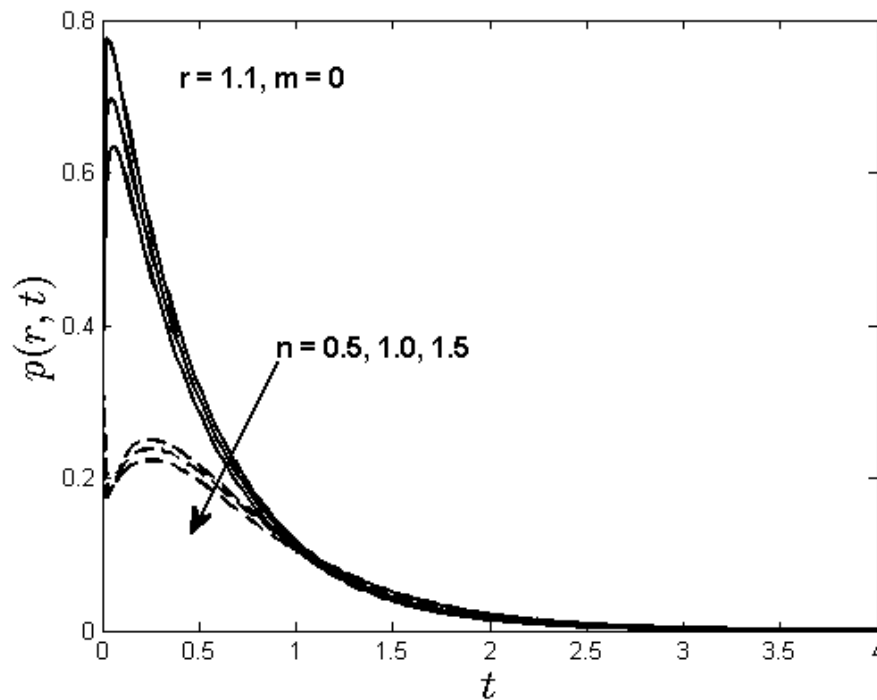


FIGURE 3.2: Power-law fluid pressure vs time for $\alpha = 1, \delta = 1, \omega = 2$. Solid lines show $g(t) = e^{-2t}$ and dashed lines indicate $g(t) = t^{\frac{1}{2}} e^{-2t}$.

Figure 3.3 describes fluid pressure $p(r, t)$ in the cavity as a function of radial distance r for different times $t = 1, 4, 7$ for shear-thinning ($n < 1$) and shear-thickening ($n > 1$) fluid for constant ($m = 0$) as well as nonlinear ($m = 3$) permeability. The range of the material constant m reported in the literature [21, 24] for biological tissues can be between 0 and 10. For the rest of the numerical computations, the following parameter values are used: $\alpha = 1, \delta = 1, \omega = 0.2, \gamma = 1, \bar{\lambda} = 0.5$ and $a(t) = 1 = g(t)$. These values are consistent with Barry and Aldis [24], since in some cases we have shown a comparison with their Newtonian case. In Figure 3.3, on the left we show shear-thinning case and on the right, we show shear-thickening case. The key observation in both cases is for large time $t = 7$, where the steady state is reached which we have shown by solid lines. The effect of nonlinear permeability is more prominent in the case of shear-thinning fluids as compared to shear-thickening fluids. The general dynamics of pressure drop is similar to that of the Newtonian case, where the nonlinear permeability case shows a slow drop off in pressure as a function of radius as compared to the linear

permeability case where the pressure drop off is faster. It is important to note that pressure p is proportional to the volume fraction ϕ , which can be seen from equation (3.31). As the solid deformation increases, so does the volume fraction of the power-law fluid, which in turn, affects the permeability of the porous medium. The increase in permeability of the porous medium creates easiness in the motion of the power-law fluid, which eventually causes pressure to drop slowly. This means that pressure drops off more slowly as we move from the constant permeability case to the nonlinear permeability case. Moreover, Figure 3.3 also suggests that from the center of the spherical cavity, pressure drops off more slowly with radial distance for shear-thickening fluids than shear-thinning fluids.

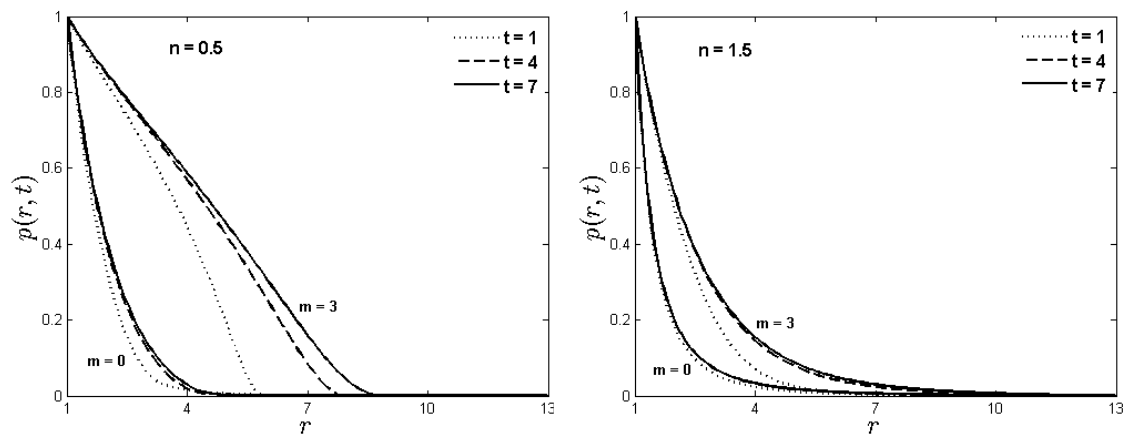


FIGURE 3.3: Left: Pressure vs radial distance for various times when $n = 0.5$; Right: Pressure vs radial distance for various times when $n = 1.5$.

The solid displacement u as a function of radial distance r at times $t = 1, 4, 7$ and permeability parameter $m = 0, 3$ for shear-thinning and shear-thickening fluids is presented in Figure 3.4. Interestingly, for linear permeability the decrease in displacement is quite uniform for both shear-thinning (shown on the left) and shear-thickening (shown on the right) fluids. When permeability is nonlinear, the shear-thinning fluid case shows a definite inflection because of non-linearities in the system similar to the Newtonian fluid case [24] whereas for shear-thickening fluids the inflection is not observed and solid displacement decays quite uniformly

but slower than the constant permeability case. This is due to the fact that shear-thickening fluid resists gradual deformation by shear stresses more than the shear-thinning fluids, which in turn, deform the porous material less as compared to the shear-thinning fluids. Moreover, for both the constant and nonlinear permeability cases, the solid displacement increase with time t for power-law fluid with more noticeable effect for shear-thinning fluids.

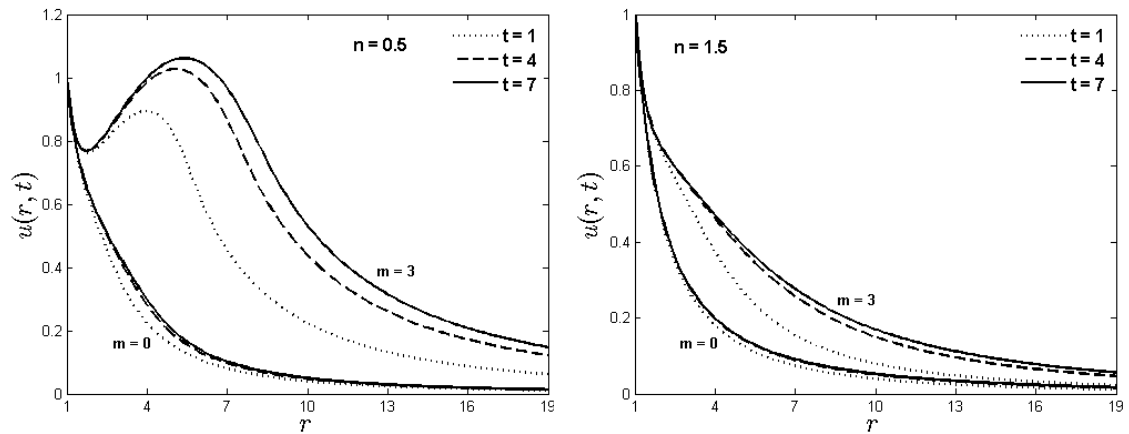


FIGURE 3.4: Left: Displacement vs radial distance for various times when $n = 0.5$; Right: Displacement vs radial distance for various times when $n = 1.5$.

When the power-law index is set to $n = 1$, the effect of absorption parameter, $\xi = \frac{\omega}{\alpha}$, on steady-state fluid pressure $p(r)$ and solid displacement $u(r)$ for the constant as well as non-linear permeability case is shown in Figure 3.5. Both graphs show that steady-state pressure and displacement increase as the parameter ξ increases for constant and non-linear permeability function. Moreover, for the same ξ , it is also observed that $p(r)$ and $u(r)$ increases as the parameter m increases, with more distinct effect for nonlinear permeability. From the graph on left, we notice that an increase in the parameter ξ magnifies the effect of nonlinearities in the system, which in turn, decreases the fluid absorption in the tissue and consequently the fluid pressure in the spherical cavity drops off more slowly for large ξ . In the figure on the right, large m and ξ contribute to the non-linearities in the system, which evidently affect the porosity of the material and produce an overall expansion of the medium despite radial compression. The inflection in the solid displacement

$u(r)$ increases as the parameter ξ increases for nonlinear permeability. Moreover, it is worth mentioning that for the Newtonian fluid case ($n = 1$), both graphs establish an excellent graphical agreement with the results of Barry and Aldis [24] for steady-state pressure and displacement as a function of radial distance for the nonlinear permeability case as indicated by the solid lines for various values of parameter ξ .

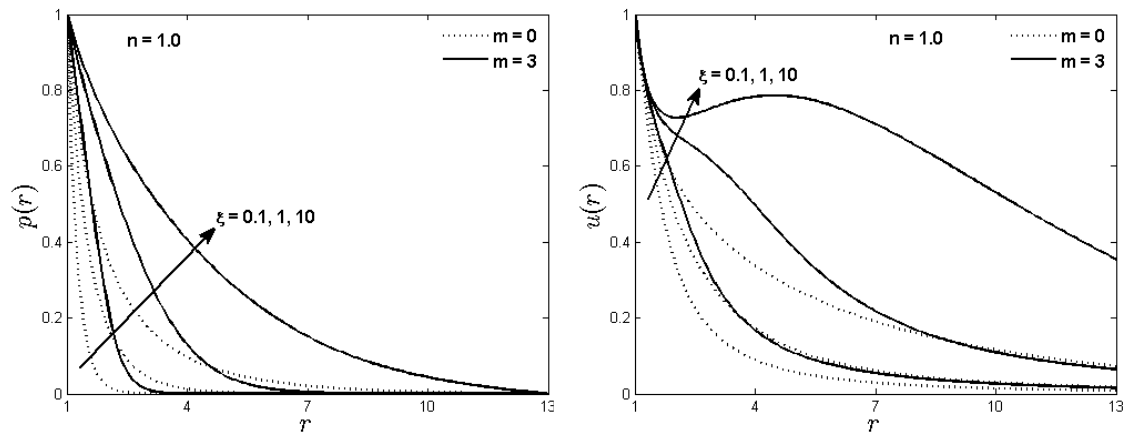


FIGURE 3.5: Left: Steady-state pressure vs radial distance for various ξ ; Right: Steady-state displacement vs radial distance for various ξ .

The effect of power-law index n on steady-state pressure and displacement is shown in Figure 3.6. The other parameter values that we have used here are $\xi = 10, 1$ and $m = 0, 3$. For the constant permeability case, the fluid pressure reaches to its steady state quickly following a uniform drop as compared to the nonlinear permeability case where we notice an exponential pressure drop. Large values of the absorption parameter ξ correspond to the higher intrinsic permeability, which shows a more dominant effect in both graphs in Figure 3.6. The decrease in ξ values decreases the effect of non-linearities in the solid displacement distribution which shows an opposite trend as compared to the large values of ξ . The inflection point that we observe in the displacement $u(r)$ shows that the porous medium is always in a state of local expansion even if the medium is compressed radially. It is evident from the graph on the right that for the constant permeability case, the solid displacement falls uniformly with the power-law index whereas in case of nonlinear permeability shear-thinning fluids exhibit greater inflection highlighting

the presence of non-linearities in the system while shear-thickening fluids show no inflection in the solid displacement even for large ξ . Thus, shear-thinning fluids induce greater solid deformation as compared to the Newtonian and shear-thickening fluids.

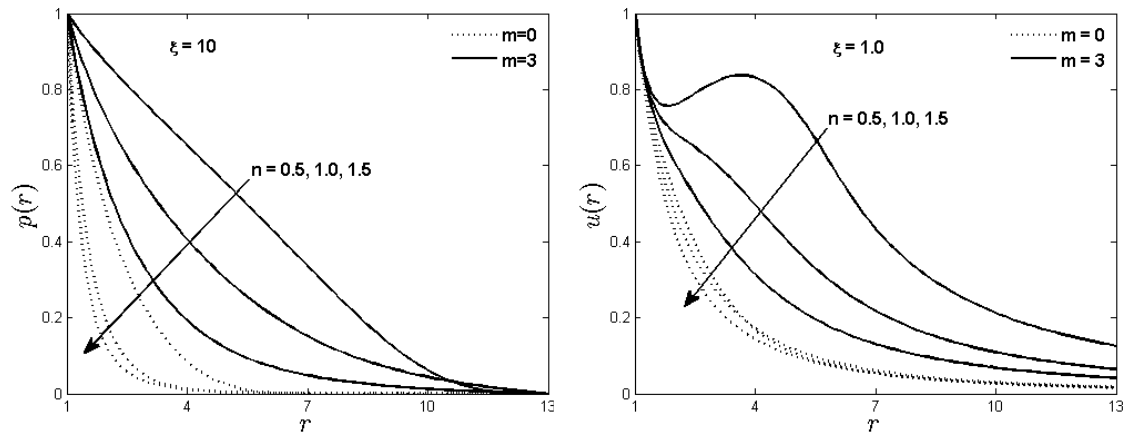


FIGURE 3.6: Left: Steady-state pressure vs radial distance for various n when $\xi = 10$; Right: Steady-state displacement vs radial distance for various n when $\xi = 1$.

The influence of power-law index n on pressure gradient $\frac{dp}{dr}$ and displacement gradient $\frac{du}{dr}$ for the case of non-linear permeability ($m = 3$) is shown in Figure 3.7. It is evident from both graphs that pressure as well as displacement gradient increase by increasing the power-law index for the larger radial distance away from center of spherical cavity. It can be seen from the figure on the right that for large values of the parameter ξ , $\frac{du}{dr} > 0$ in a small region close to spherical cavity but not adjacent to it. This region is found larger for shear-thinning fluids than Newtonian and shear-thickening fluids. This means that in some porous materials non-linearities are sufficient to produce an expansion in the annular as well as radial directions and this effect may be useful in various industrial applications.

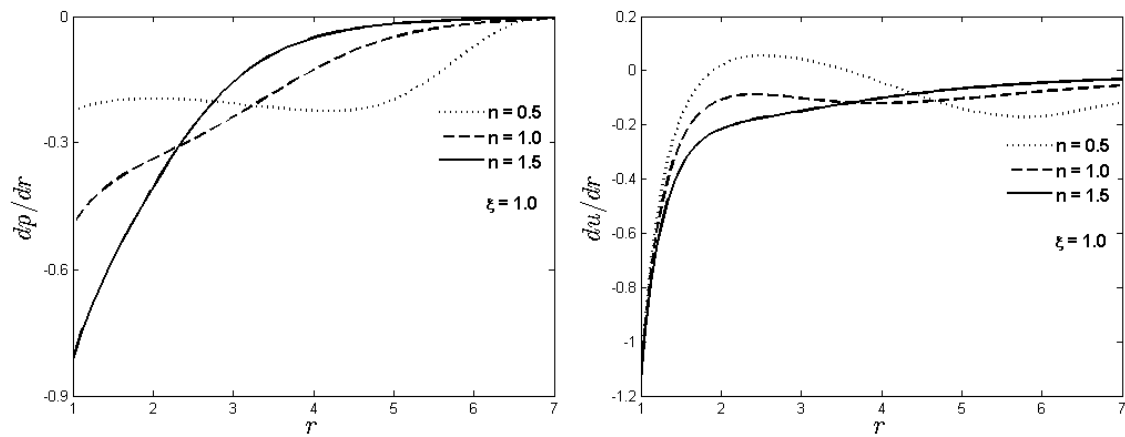


FIGURE 3.7: Left: Steady-state pressure gradient vs radial distance for various n when $m = 3$; Right: Steady-state displacement gradient vs radial distance for various n when $m = 3$.

Finally, the effect of power-law index n on tissue permeability expressed in equation (3.33) is presented in Figure 3.8. The tissue permeability, which is a measure of the ability of a porous material to allow fluid to pass through it, is found more for shear-thinning fluids in comparison to Newtonian and shear-thickening fluids. This is because of the fact that shear-thinning fluids are less viscous (i.e. viscosity decreases with applied shear stress) and experience less resistance in the flow which enable them to pass in more quantity through the tissue than shear-thickening fluids. This effect serves as a justification for the reduction of fluid pressure and hence the solid displacement of the porous tissue with the power-law index.

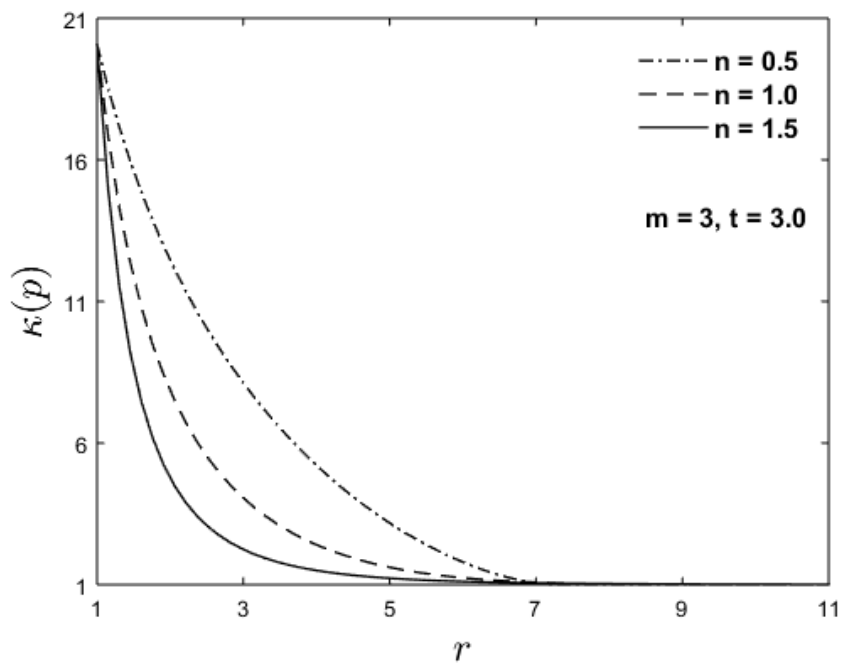


FIGURE 3.8: Pressure-dependent permeability vs radial distance for various n when $m = 3, t = 3$.

3.5 Conclusion

In this chapter, we have analyzed non-Newtonian flow-induced deformation in absorbing porous biological tissues modeled as a nonlinear deformable porous material by using the continuum mixture theory approach. The soft tissue was assumed to be isotropic, homogeneous and linearly elastic. A nonlinear diffusion equation in terms of power-law fluid pressure and a relation for the solid displacement of the tissue was obtained as a consequence of mathematical modeling of a spherical cavity embedded in an infinite porous medium. The governing equations for the fluid pressure and solid displacement were solved numerically for the non-Newtonian fluid case. In particular, Matlab's solvers *pdepe* and *bvp4c* were utilized to solve the pressure equation for the unsteady and steady-state case, respectively whereas trapezoidal rule of numerical integration was employed to get the solution for the solid displacement profile.

Our solutions indicate that porosity of the tissue is increased due to annular expansion and in highly non-linear situations a radial expansion can result as well. This expansion of the porous material increases the fluid absorption in the biological tissue which is observed more for shear-thinning fluids than shear-thickening fluids. The increase in the permeability of the absorbing porous tissue causes more fluid to seep through the tissue with less resistance. The power-law fluid pressure and the solid displacement profiles were found to increase with time, permeability and absorption parameter for both the steady and unsteady situations. The large values of the permeability and absorption parameters correspond to the presence of non-linearities in the system which enhance the fluid pressure and solid displacement of the tissue. It was also shown that permeability of the tissue decreases by increasing the power-law index and this effect causes the fluid pressure in the tissue and hence the solid displacement to decay more slowly for shear-thinning fluids as compared to shear-thickening fluids.

Chapter 4

Application of Magnetic Field to Flow Induced-Deformation in Absorbing Porous Tissues

4.1 Introduction

Based on the geometry of the previous chapter, the effect of a uniform applied magnetic field on the flow-induced deformation in the absorbing porous biological tissues has been investigated in this chapter. Specifically, a model with a spherical cavity embedded in a porous medium of infinite extent has been used to find fluid pressure and the solid displacement of the tissue as a function of radial distance and time. The governing set of equations is non-dimensionalized using some suitable dimensionless variables. The method of lines approach is used to numerically solve a one-dimensional partial differential equation in terms of fluid pressure whereas the solid displacement is computed numerically using the trapezoidal rule. The effect of magnetic parameter on fluid pressure, solid displacement and tissue permeability is illustrated graphically.

In Section 4.2, the mathematical formulation of the problem using the continuum mixture theory approach is presented. Solution methodology is presented in Section 4.3. The results are included in Section 4.4 with an appropriate discussion followed by the concluding remarks in the last Section 4.5.

4.2 Mathematical Formulation

Based on the geometry of the problem considered in the preceding chapter, we develop a model of flow-induced deformation in absorbing porous tissues subject to a uniform radial magnetic field as shown in Figure 4.1. The orientation of the applied magnetic field is taken in such a way that it produces a radial flow in the tissue. The soft porous tissue containing a spherical cavity is considered to be a binary mixture of an organic solid and a conducting fluid.

We assume that the injected fluid in the porous tissue is conducting and viscous while the organic solid matrix is isotropic, homogeneous and linearly elastic. The gravitational and osmotic forces are neglected and the solid deformation is supposed to be small. It is also supposed that the shear stresses are negligible on account of one dimensional radial flow and the constituents of the mixture are intrinsically incompressible. Under these assumptions, the equations of motion for solid and fluid phase are written in scalar form as (see Appendix A for details)

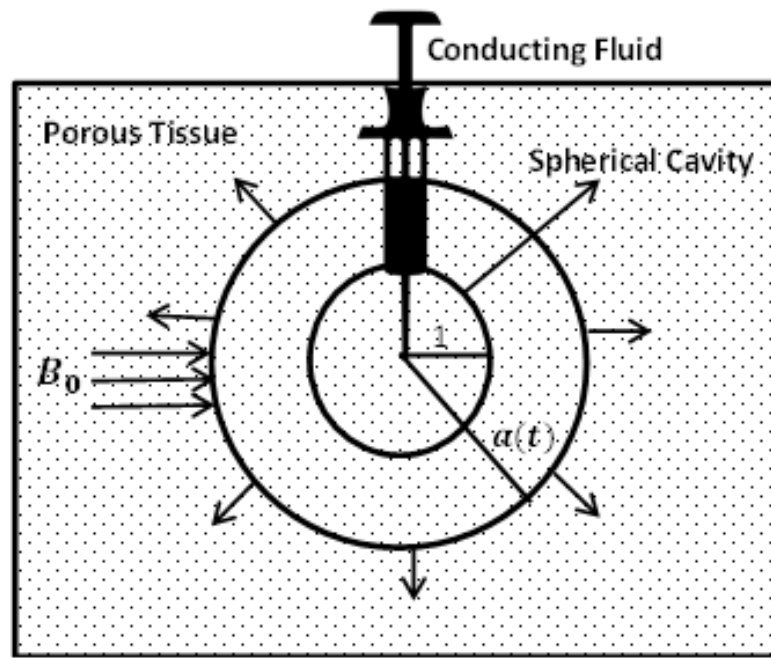


FIGURE 4.1: Schematic of MHD fluid flow from an injection site into a porous medium. Growth of the cavity from radius 1 to $a(t)$ is indicated.

$$\frac{\partial \phi^s}{\partial t} + \frac{1}{r^2} \frac{\partial}{\partial r} (r^2 \phi^s v^s) = 0, \quad (4.1)$$

$$\frac{\partial \phi^\ell}{\partial t} + \frac{1}{r^2} \frac{\partial}{\partial r} (r^2 \phi^\ell v^\ell) = -\frac{\beta}{\rho_T^\ell} p, \quad (4.2)$$

$$v^s - v^\ell = \frac{\phi^\ell}{K} \frac{\partial p}{\partial r} - \frac{\sigma_0 B_0^2}{K} v^s, \quad (4.3)$$

$$\frac{\partial \sigma_{rr}}{\partial r} + 2 \frac{\sigma_{rr} - \sigma_{\theta\theta}}{r} = \frac{\partial p}{\partial r}, \quad (4.4)$$

where ϕ^s and ϕ^ℓ represent solid and fluid volume fractions and v^s and v^ℓ are velocities of solid and fluid phase, respectively, ρ_T^ℓ is the intrinsic density of fluid phase, β is the proportionality constant which depends upon the concentration of capillaries and lymphatics in the tissue and permeability of their walls, p is the fluid pressure, K the drag coefficient of relative motion, σ_0 the electric conductivity of the fluid, B_0 the uniform magnetic flux. It is important to note that the last term on right hand side of equation (4.3) is the contribution of MHD and left hand side of equation (4.4) is the divergence of solid stress in the radial direction where σ_{rr}

and $\sigma_{\theta\theta} = \sigma_{\phi\phi}$ are defined as components of solid stress. Equations (4.1) and (4.2) represent the mass balance relations for solid and fluid phase, respectively, whereas equations (4.3) and (4.4) are derived from solid and fluid momentum balances [69, 70]. The term appearing on right hand side of equation (4.2) is due to loss of fluid mass at a rate proportional to fluid pressure while it passes through capillaries and lymphatics. Adding equations (4.1) and (4.2), we obtain

$$\frac{\partial}{\partial t}(\phi^s + \phi^\ell) + \frac{1}{r^2} \frac{\partial}{\partial r} \left(r^2 (\phi^s v^s + \phi^\ell v^\ell) \right) = -\frac{\beta}{\rho_T^{\ell}} p, \quad (4.5)$$

which on denoting the macroscopic medium velocity in the radial direction, $v_r = \phi^s v^s + \phi^\ell v^\ell$, and using the relation, $\phi^s + \phi^\ell = 1$, reduces to

$$\frac{1}{r^2} \frac{\partial}{\partial r} (r^2 v_r) = -\frac{\beta}{\rho_T^{\ell}} p. \quad (4.6)$$

Using equation (4.4) into (4.3) and simplifying, yields

$$\frac{\partial \sigma_{rr}}{\partial r} + 2 \frac{\sigma_{rr} - \sigma_{\theta\theta}}{r} = \frac{K}{\phi^\ell} (v^s - v^\ell) + \frac{\sigma_0 B_0^2}{\phi^\ell} v^s. \quad (4.7)$$

Denoting $v^s = \frac{\partial u}{\partial t}$, where u is a component of solid displacement and using an expression for v^ℓ from macroscopic medium velocity v_r into the relation (4.7) and keeping in view equation (4.4), we have

$$\frac{\partial p}{\partial r} = \frac{\partial \sigma_{rr}}{\partial r} + 2 \frac{\sigma_{rr} - \sigma_{\theta\theta}}{r} = \frac{1}{\kappa(\phi)} \left(\frac{\partial u}{\partial t} - v_r \right) + \frac{\sigma_0 B_0^2}{\phi^\ell} \frac{\partial u}{\partial t}, \quad (4.8)$$

where

$$\kappa(\phi) = \frac{(\phi^\ell)^2}{K}, \quad (4.9)$$

is defined to be the permeability of the medium [24]. Equation (4.8) can be explained physically by taking into account the Darcy's law and considering the solid stress as being governed by the standard equilibrium equation of the theory of linear elasticity. As suggested by the relation (4.9), the permeability κ of the porous medium decreases as a consequence of solid compression. Taking into

account equation (4.4) and the relation $\frac{\partial \sigma_{rr}}{\partial r} + 2\frac{\sigma_{rr} - \sigma_{\theta\theta}}{r} = H_a \frac{\partial \phi}{\partial r}$ where $H_a = \lambda + 2\mu$ is the aggregate modulus and (λ, μ) are Lamé constants (see Appendix for details), the governing equation (4.8) can be written as

$$\frac{\partial p}{\partial r} = H_a \frac{\partial \phi}{\partial r} = \frac{1}{\kappa(\phi)} \left(\frac{\partial u}{\partial t} - v_r \right) + \frac{\sigma_0 B_0^2}{\phi^\ell} \frac{\partial u}{\partial t}, \quad (4.10)$$

which on equating the first two expressions and then integrating gives the relationship between p and ϕ as

$$p(r, t) = H_a \phi(r, t), \quad (4.11)$$

where both p and ϕ tend to zero as $r \rightarrow \infty$. From equations (4.10) and (4.11), a relation for v_r in terms of fluid pressure p and solid displacement u may be obtained as

$$v_r(r, t) = \frac{\partial u}{\partial t} - \left(\kappa \left(\frac{p}{H_a} \right) \frac{\partial p}{\partial r} \right) + \frac{\kappa \left(\frac{p}{H_a} \right) \sigma_0 B_0^2}{\phi^\ell} \frac{\partial u}{\partial t}. \quad (4.12)$$

Combining equations (4.6) and (4.12), we obtain

$$\begin{aligned} & \frac{1}{r^2} \frac{\partial}{\partial r} \left(r^2 \frac{\partial u}{\partial t} \right) - \frac{1}{r^2} \frac{\partial}{\partial r} \left\{ r^2 \kappa \left(\frac{p}{H_a} \right) \frac{\partial p}{\partial r} \right\} + \frac{1}{r^2} \frac{\partial}{\partial r} \left(r^2 \frac{\kappa \left(\frac{p}{H_a} \right) \sigma_0 B_0^2}{\phi^\ell} \frac{\partial u}{\partial t} \right) \\ & = - \frac{\beta}{\rho_T^\ell} p. \end{aligned} \quad (4.13)$$

As the porous tissue is compressed, consequently its permeability would reduce due to a decrease in porosity. The relationship between porosity and displacement of the medium is given by [24]

$$1 - \phi^\ell = \frac{\phi_0^s}{\sqrt{\det \mathbf{G}}}, \quad (4.14)$$

where \mathbf{G} is the left Cauchy-Green deformation tensor and ϕ_0^s is the initial solid volume fraction. For infinitesimal solid deformations this can be approximated

as [24, 71]

$$\phi^\ell = \phi_0^\ell + \phi_0^s \nabla \cdot \mathbf{u} = \phi_0^\ell (1 + \alpha_0 \phi), \quad (4.15)$$

where $\phi = \nabla \cdot \mathbf{u}$ is the one-dimensional dilatation and $\alpha_0 = \frac{\phi_0^s}{\phi_0^\ell}$. The permeability as a function of porosity can then be expressed as $\kappa = \kappa(\phi)$ which is related to fluid pressure via equation (4.11). Recognizing the first term on left hand side of equation (4.13) as the time derivative of $\phi = \frac{1}{r^2} \frac{\partial}{\partial r} (r^2 u)$ and keeping in view the relation (4.11), we obtain

$$\frac{1}{H_a} \frac{\partial p}{\partial t} - \frac{1}{r^2} \frac{\partial}{\partial r} \left\{ r^2 \kappa \left(\frac{p}{H_a} \right) \frac{\partial p}{\partial r} \right\} + \frac{1}{r^2} \frac{\partial}{\partial r} \left(r^2 \frac{\kappa \left(\frac{p}{H_a} \right) \sigma_0 B_0^2}{\phi^\ell} \frac{\partial u}{\partial t} \right) = -\frac{\beta}{\rho_T^\ell} p. \quad (4.16)$$

This equation is expressed in terms of fluid pressure p except the third term on left hand side which still involves solid displacement component u in the parenthesis. In order to eliminate u from equation (4.16), we in view of relations (4.11) and (4.15) assume a linear permeability of the form

$$\kappa(\phi) = k_0(1 + m\phi), \quad (4.17)$$

where k_0 and m are material constants. Note that this simple form of permeability, which is a general approximation to any $\kappa(\phi)$ for small ϕ , is valid for infinitesimal solid deformations and various authors [17, 66] have considered a similar form to study the water flow through arterial tissue and radial flow through deformable porous shells. Using the relations (4.11), (4.15) and (4.17) into the governing equation (4.16), we obtain

$$\begin{aligned} & \frac{1}{H_a} \frac{\partial p}{\partial t} - \frac{1}{r^2} \frac{\partial}{\partial r} \left\{ r^2 k_0 \left(1 + m \frac{p}{H_a} \right) \frac{\partial p}{\partial r} \right\} + \frac{1}{r^2} \frac{\partial}{\partial r} \left\{ r^2 \frac{k_0 \left(1 + m \frac{p}{H_a} \right) \sigma_0 B_0^2}{\phi_0^\ell \left(1 + \alpha_0 \frac{p}{H_a} \right)} \frac{\partial u}{\partial t} \right\} \\ & = -\frac{\beta}{\rho_T^\ell} p. \end{aligned} \quad (4.18)$$

Assuming initial fluid volume fraction ϕ_0^ℓ to be constant and $m = \alpha_0$, this equation can be reduced to a more convenient form as

$$\frac{1}{H_a} \left(1 + \frac{k_0 \sigma_0 B_0^2}{\phi_0^\ell} \right) \frac{\partial p}{\partial t} - \frac{k_0}{r^2} \frac{\partial}{\partial r} \left\{ r^2 \left(1 + m \frac{p}{H_a} \right) \frac{\partial p}{\partial r} \right\} = - \frac{\beta}{\rho_T^\ell} p. \quad (4.19)$$

This equation may be non-dimensionalized using the following dimensionless quantities

$$\bar{t} = \frac{t}{t_0}, \quad \bar{r} = \frac{r}{r_0}, \quad \bar{p} = \frac{p}{p_0}, \quad \bar{u} = \frac{u}{u_0}, \quad (4.20)$$

where t_0, r_0, p_0 and u_0 are typical time, radius, pressure and deformation scales, respectively. After introducing these choices, equation (4.19) on dropping the bars takes the following form

$$\frac{\partial p}{\partial t} = \frac{\alpha}{1+M} \frac{1}{r^2} \frac{\partial}{\partial r} \left\{ r^2 (1 + m \delta p) \frac{\partial p}{\partial r} \right\} - \frac{\omega}{1+M} p, \quad (4.21)$$

where various dimensionless parameters are defined as

$$\alpha = \frac{H_a t_0 k_0}{r_0^2}, \quad \delta = \frac{p_0}{H_a}, \quad \omega = \frac{\beta H_a t_0}{\rho_T^\ell}, \quad M = \frac{k_0 \sigma_0 B_0^2}{\phi_0^\ell}. \quad (4.22)$$

Note that values of various parameters appearing in this equation may differ considerably among biological tissues [24]. The equation (4.21) is required governing equation in terms of non-dimensional fluid pressure $p(r, t)$ under the action of a uniform applied magnetic field and is related to porosity ϕ via equation (4.11). This parabolic PDE is nonlinear which makes it difficult to solve analytically. We thus use a numerical method for its solution described in the next section. It is worth mentioning that setting the magnetic parameter $M = 0$ in equation (4.21) and assuming a linear permeability of the form (4.17), we recover the Newtonian fluid case [24]. A natural time scale t_0 for the current problem may be obtained by setting $\frac{\alpha}{1+M} = 1$ as

$$t_0 = \frac{r_0^2}{H_a k_0} \left(1 + \frac{k_0 \sigma_0 B_0^2}{\phi_0^\ell} \right), \quad (4.23)$$

which reduces the parameter ω in equation (4.22) to

$$\omega = \frac{\beta r_0^2}{\rho_T^\ell k_0} \left(1 + \frac{k_0 \sigma_0 B_0^2}{\phi_0^\ell} \right). \quad (4.24)$$

The non-dimensional boundary conditions for fluid pressure $p(r, t)$ and solid displacement $u(r, t)$ in the tissue from the preceding chapter are rewritten as

$$p(r, 0) = f(r), \quad p(a, t) = g(t), \quad p(r, t) \rightarrow 0 \quad \text{as } r \rightarrow \infty, \quad (4.25)$$

and

$$\left[\frac{\partial u}{\partial r} + 2\bar{\lambda} \frac{u}{r} \right]_{r=a} = 0, \quad u(r, t) \rightarrow 0 \quad \text{as } r \rightarrow \infty, \quad (4.26)$$

where $f(r)$ and $g(t)$ are some specified functions of their arguments and $\bar{\lambda} = \frac{\lambda}{\lambda + 2\mu}$. Note that the given displacement boundary condition for infinitesimal deformation was derived from a general boundary condition between a fluid and a porous material [68]. Since the governing equation (4.21) is solved for fluid pressure, therefore an equation is required that relates solid displacement to fluid pressure. This is accomplished by combining the relations $\phi = \frac{1}{r^2} \frac{\partial}{\partial r}(r^2 u)$ and $p(r, t) = H_a \phi(r, t)$ with equation (4.20) to give

$$p(r, t) = \frac{1}{\gamma r^2} \frac{\partial}{\partial r}(r^2 u), \quad (4.27)$$

where $\gamma = \frac{\rho_0 r_0}{H_a u_0}$ is a dimensionless parameter. Integrating this equation and applying the boundary conditions (4.26) for solid displacement, yields

$$u(r, t) = \frac{\gamma}{r^2} \left\{ \int_{a(t)}^r s^2 p(s, t) ds + \frac{a^3(t)g(t)}{2(1 - \bar{\lambda})} \right\}, \quad (4.28)$$

which gives displacement of solid as a function of non-dimensional radial distance r and time t . Note that the effect of magnetic parameter on steady-state solutions is absent as suggested by equation (4.21). In order to carry out numerical computations for the nonlinear problem, we assume that $a(t) = 1, g(t) = 1, f(r) = 0, \alpha = 1, \gamma = 1, \bar{\lambda} = 0.5$ and $\delta = 1$, which are consistent with the values considered

in [24].

4.3 Solution Methodology

In this section, we briefly outline the procedure for the solution of governing set of equations. To begin with, we first give an exact solution of equation (4.21) in terms of MHD fluid pressure $p(r, t)$ subject to boundary conditions (4.25) for the constant permeability case (i.e. $m = 0$) and compare the result with method of lines (MOL) as a validation of numerical scheme to be employed for the solution of nonlinear problem. Following the method adopted by Barry and Aldis [24] for linearized problem, the solution for fluid pressure for the choice of applied pressure, $g(t) = e^{\frac{-\omega}{1+M}t} t^{\frac{m}{2}}$, is given as

$$p(r, t) = \frac{a}{r} e^{\frac{-\omega}{1+M}t} (4t)^{\frac{m}{2}} \mathbf{i}erfc\left(\frac{r-a}{2\sqrt{\frac{\alpha t}{1+M}}}\right) \Gamma\left(1 + \frac{m}{2}\right), \quad (4.29)$$

where m is a non-negative integer, $\Gamma(\cdot)$ is the gamma function and $\mathbf{i}erfc$ represents integration of the error function [72]. As stated earlier, for the nonlinear problem we use method of lines whose main idea is to discretize the space variable and its derivatives and leaving the time variable continuous [73]. This space discretization results into a system of coupled ODEs which may then be solved using Matlab's well established and efficient solvers as an initial value problem. For completeness, we now show a brief calculation of the MOL by discretizing the governing equation (4.21) using central finite difference formulas for the first and the second space derivatives as

$$\begin{aligned} \frac{dp_i}{dt} = & \frac{\alpha}{1+M} \left[\frac{2(1+m\delta p_i)}{a+(i-1)dr} \left(\frac{p_{i+1}-p_{i-1}}{2dr} \right) + m\delta \left(\frac{p_{i+1}-p_{i-1}}{2dr} \right)^2 + \right. \\ & \left. (1+m\delta p_i) \left(\frac{p_{i+1}-2p_i+p_{i-1}}{(dr)^2} \right) \right] - \frac{\omega}{1+M} p_i, \end{aligned} \quad (4.30)$$

where

$$i = 1, 2, 3, \dots, N, \quad p_i = p(r_i, t), \quad r_i = a + (i - 1)dr, \quad dr = \frac{b - a}{N}. \quad (4.31)$$

From the boundary conditions (4.25) for fluid pressure, we have

$$p_0 = g(t), \quad p_{N+1} = 0, \quad p(r_i, 0) = f(r_i), \quad (4.32)$$

where p_0 and p_{N+1} represent, respectively, the left boundary and right boundary value of fluid pressure and $p(r_i, 0)$ are the initial conditions for the discretized problem. We thus have an initial value problem consisting of N number of ODEs in equation (4.30) and corresponding initial conditions outlined in equation (4.32), which may now be solved using efficient Matlab's solver such as *ode23s*. It is important to note that in order to carry out numerical simulations, we truncate the spatial domain for fluid pressure at $r = 13$ due to satisfaction of the far field boundary condition and the temporal domain at $t = 7$ because after this value there is no significant change in the fluid pressure and hence the long time behavior of the solution may be obtained. Moreover, solid displacement $u(r, t)$ in equation (4.28) is computed using trapezoidal rule by solving a definite integral involving fluid pressure. It is also important to note that in the implementation of numerical method for the nonlinear problem the left boundary condition was applied at non-dimensional radius $r = 1$ corresponding to initial radius.

Figure 4.2 presents a comparison between the exact (i.e. equation (4.29)) and numerical (i.e. equation (4.30)) solution for the non-dimensional fluid pressure in the presence of magnetic field for the constant permeability case. An excellent agreement between the two solutions is observed validating the proposed numerical scheme.

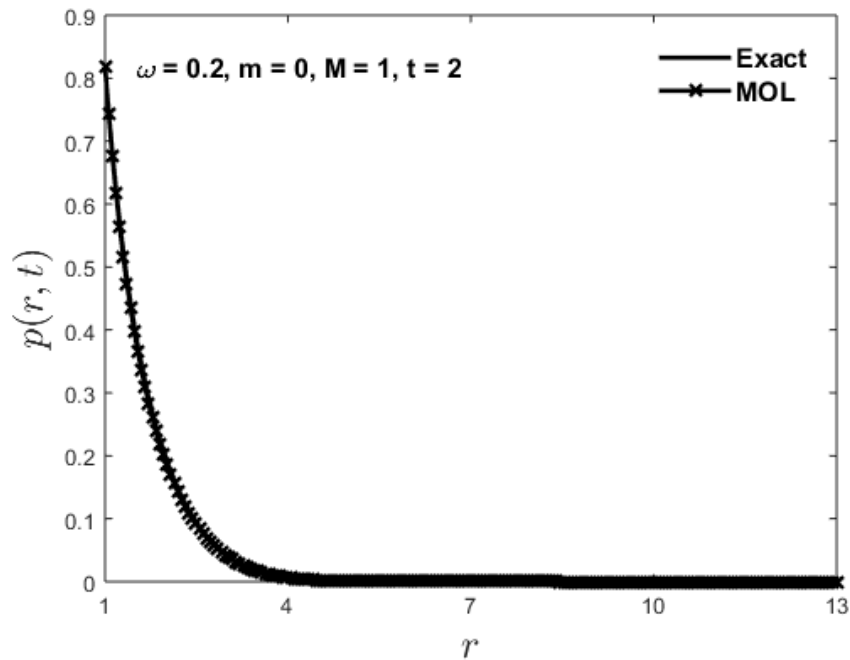


FIGURE 4.2: A comparison between the exact and numerical solution for fluid pressure when $m = 0$.

4.4 Results and Discussion

This section contains the outcome of our numerical simulations for fluid pressure and solid displacement for various values of emerging parameters. Methods described in the previous section are used and the results are illustrated graphically.

In Figure 4.3, non-dimensional fluid pressure $p(r, t)$ is plotted against time t for the choice of four different applied pressure profiles $g(t)$. The solid curve on the graph indicates that fluid pressure in the tissue drops off exponentially with time whereas the dashed curve suggests that there is an initial increase in the pressure to a local maximum followed by an exponential decay. These two applied pressure profiles were also considered by Barry and Aldis [24]. Moreover, the dashed-dotted curve on this graph representing a periodic form of applied pressure shows that fluid pressure in the porous tissue rises initially to a maximum value followed by a periodic decrease while the dotted curve representing a quadratic type of applied pressure indicates that pressure of fluid in the tissue is increasing from the center

of the cavity. It is to be noted that similar form of periodic and quadratic pressure was also considered in [74].

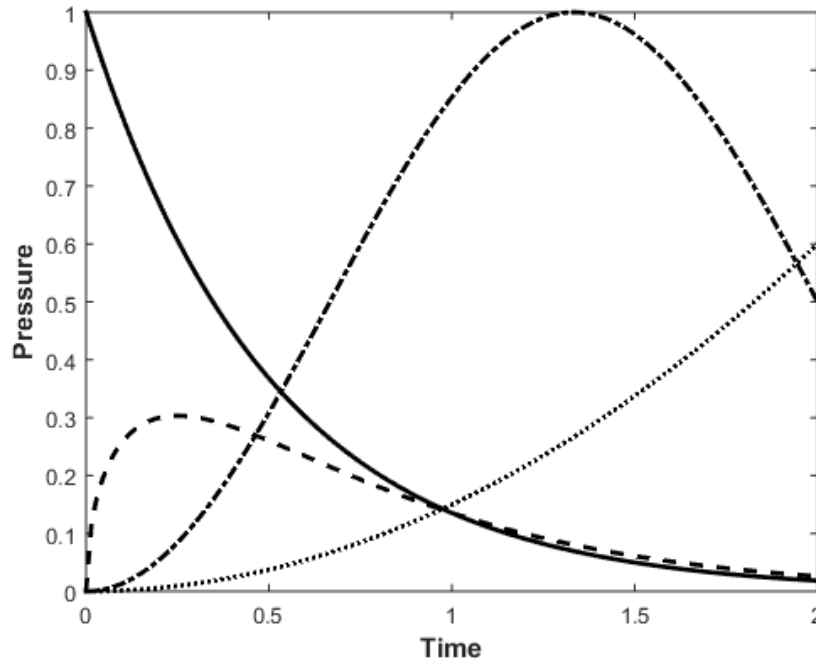


FIGURE 4.3: Fluid pressure vs time for various $g(t)$. Solid line: $g(t) = e^{-2t}$, Dashed line: $g(t) = t^{\frac{1}{2}}e^{-2t}$, Dashed-dotted line: $g(t) = 0.5(1 - \cos(0.75\pi t))$, Dotted line: $g(t) = 0.15t^2$.

Figure 4.4 describes the influence of magnetic parameter M on fluid pressure $p(r, t)$ at $t = 0.5, 7.0$ for a given distance from center of the cavity. This graph shows that fluid pressure in the tissue drops off more rapidly as strength of the magnetic field increases. The Lorentz force associated with applied magnetic field boosts the fluid flow in the tissue which consequently reduces fluid pressure in the porous material. Thus, application of a suitably designed magnetic field may possibly assist to control the fluid flow in deformable porous tissues for practical purposes. On the other hand, for fixed M , fluid pressure in the tissue rises with time and there is not much difference in pressure distribution after $t \geq 7$ explaining the long time behavior of the solution. Since fluid pressure and porosity of the tissue are related directly via equation (4.11), so this plot also illustrates the porosity as a function of radial distance and time.

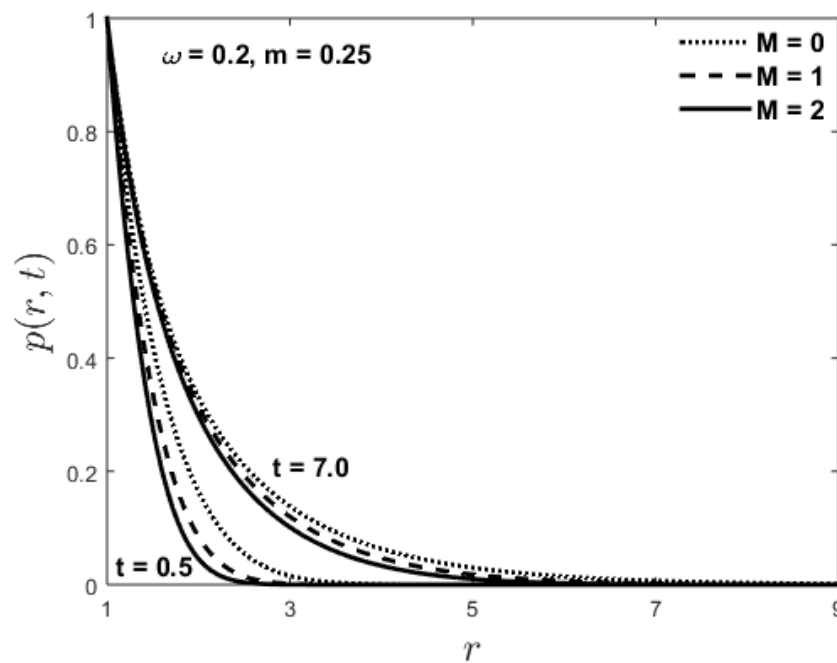


FIGURE 4.4: Fluid pressure vs radial distance for various M at $t = 0.5, 7.0$.

The effect of magnetic parameter M on solid displacement $u(r, t)$ at $t = 0.5, 7.0$ is presented in Figure 4.5. The relation for solid displacement (4.28) suggests that higher fluid pressure in the tissue should induce greater solid deformation, and vice versa. Accordingly, due to a reduction in fluid pressure with magnetic parameter, the tissue solid displacement also decays with magnetic parameter as shown in Figure 4.5. This means that a properly applied high magnetic field can prevent large solid deformation of the material. Additionally, this graph also illustrates that deformation of the solid increases with time, and that after $t \geq 7$, there is not significant change in the displacement distribution of the tissue. Moreover, in the absence of magnetic effects (i.e. $M = 0$) and for large m , it is expected that solid displacement u would exhibit greater inflection due to nonlinearities in the system, particularly, for large time.

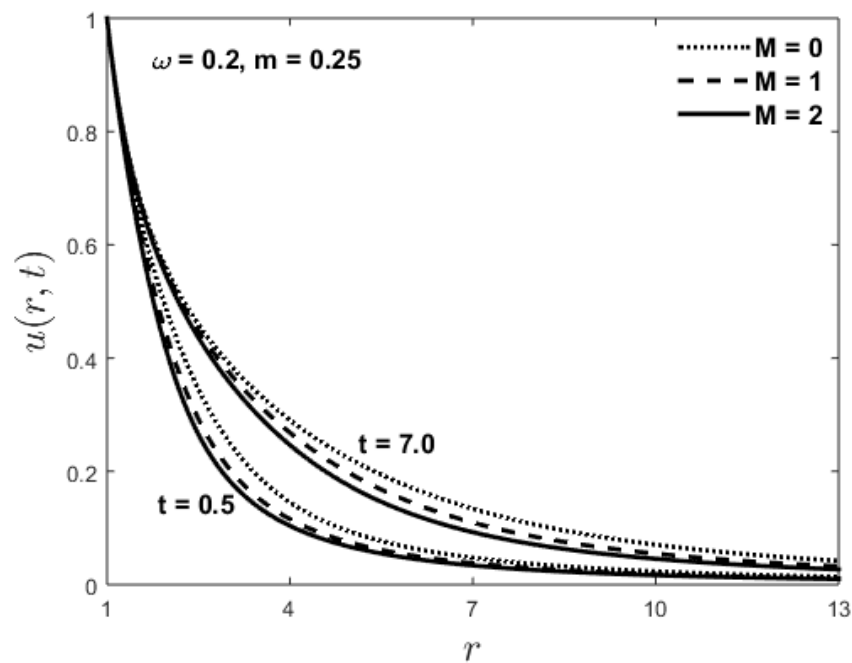


FIGURE 4.5: Solid displacement vs radial distance for various M at $t = 0.5, 7.0$.

The pressure-dependent permeability, $\kappa = 1 + m\delta p$, is plotted against radial distance r in Figure 4.6 for different values of magnetic parameter M when $m = 0.25$ and $\delta = 1$. The tissue permeability reduces as strength of transversely applied magnetic field increases validating the direct relation with fluid pressure. This fact indicates that a high magnetic field would allow less fluid to seep through the porous tissue.

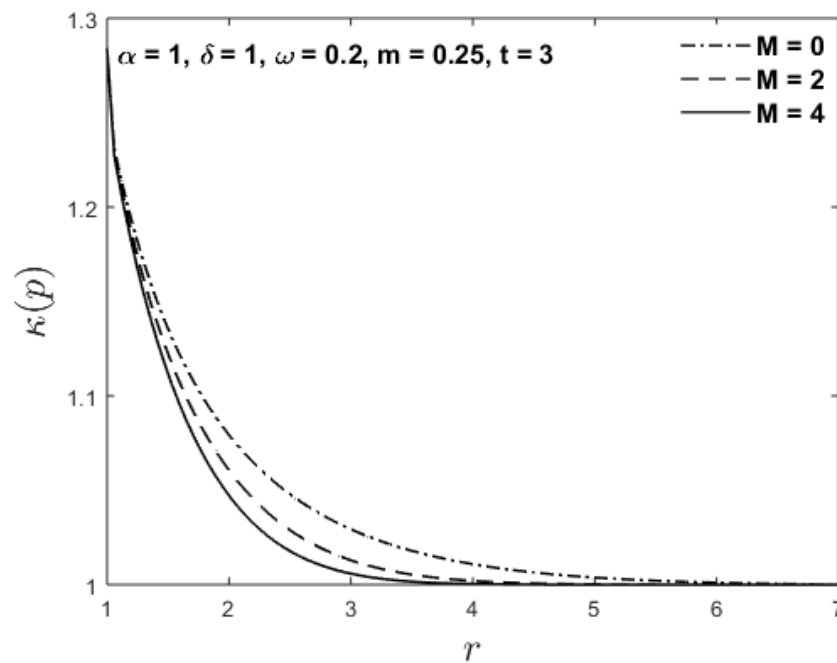


FIGURE 4.6: Pressure-dependent permeability $\kappa(p) = 1 + m\delta p$ vs radial distance for various M when $m = 0.25$ and $\delta = 1$.

Finally, influence of the parameter ω on unsteady fluid pressure and solid displacement in the absence and presence of magnetic field is illustrated in Figures 4.7 and 4.8, respectively. The fluid pressure in porous tissue decreases as more fluid is absorbed with more profound effect in the absence of magnetic field. This effect is consistent with variation of fluid pressure due to fluid flow in porous materials. The application of magnetic field allows fluid pressure to drop more rapidly even for higher fluid absorption rate. A similar behavior of solid displacement is noted for the parameter ω in Figure 4.8. Moreover, from these two graphs, it appears that higher fluid pressure causes greater solid deformation suggesting a direct relation between the two quantities.

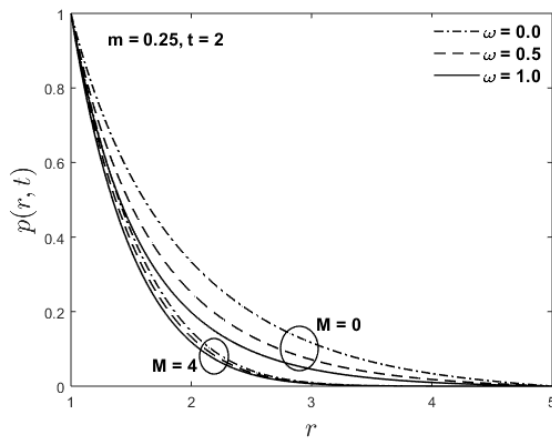


FIGURE 4.7: Fluid pressure vs radial distance for various ω when $m = 0.25, t = 2$.

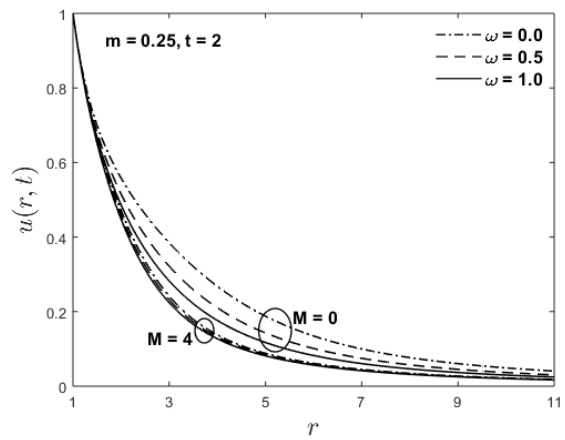


FIGURE 4.8: Solid displacement vs radial distance for various ω when $m = 0.25, t = 2$.

4.5 Concluding Remarks

In this study, we analyzed a one-dimensional model of flow-induced deformation from pressurized spherical cavities in absorbing porous tissues under an applied magnetic field. The deformable porous tissue was assumed to be isotropic, homogeneous and linearly elastic. The continuum mixture theory was used to develop the model assuming solid deformation to be infinitesimally small. A linear permeability relation was considered which allowed the governing equation to be written explicitly in terms of fluid pressure. A method of lines approach was adopted to solve the nonlinear parabolic PDE in terms of fluid pressure which was then used to find tissue solid displacement by employing the trapezoidal rule.

We noticed a reasonable reduction in fluid pressure, solid displacement and permeability of the tissue due to the presence of magnetic effects. Thus, a properly designed magnetic field may help achieve the required fluid flow and solid deformation in the tissue for certain physiological applications. The solid deformation enhances fluid absorption in the tissue and alters the porosity and permeability of the material. Although, we assumed that the absorption rate and tissue pressure

are related linearly, however, more sophisticated forms of the absorption process may be considered to enhance the understanding of these complex systems.

This work is relevant to the interpretation of experimental studies on neuropharmacology and in situ electrochemistry, especially with MHD effects. Other applications include the activation and magnetization of a variety of soft tissues for clinical purposes. Finally, it is worth mentioning that within the framework of mixture theory for modeling multiphase systems, a small extension can reveal interesting physical features despite the resulting nonlinearity of the governing system of equations.

Chapter 5

Ion-Induced Deformation of Articular Cartilage with Strain-Dependent Nonlinear Permeability and MHD Effects

5.1 Introduction

The aim of this chapter is to examine the effects of the applied magnetic field and strain-dependent nonlinear permeability on the deformation of articular cartilage equilibrated in a sodium chloride solution. A thin rectangular specimen of bovine cartilage is considered which is assumed to be isotropic and linearly elastic solid. A biphasic mixture theory approach has been employed to model the nonlinear deformable porous medium in the presence of a change in the ion concentration of the bathing solution. The governing set of coupled equations in terms of ion concentration, solid displacement, and fluid pressure are non-dimensionalized using appropriate dimensionless quantities. Analytical solutions are provided for the constant permeability case whereas for the nonlinear permeability case the displacement equation is solved numerically using the method of lines. The effect

of various emerging parameters such as magnetic and permeability parameters on the displacement and pressure profiles is illustrated graphically. Moreover, in some cases, a graphical comparison to the previously published results is also provided.

In Section 5.2, a mathematical model using biphasic mixture theory is introduced. The solution procedure is explained in Section 5.3 followed by results and discussion in Section 5.4. In the last section, the concluding remarks are presented.

5.2 Mathematical Modeling

We consider a small rectangular specimen of bovine articular cartilage in a continuous supply of sodium chloride (NaCl) salt solution under the action of a uniform applied magnetic field as shown in Figure 5.1. The typical length, width and thickness of the sample tissue are taken as $1.5 \times 10^{-2}m$, $1.7 \times 10^{-3}m$ and $2 \times 10^{-4}m$, respectively [37]. We consider a Cartesian geometry where the coordinates x, y, z are taken along the height (or thickness), width and the length directions, respectively.

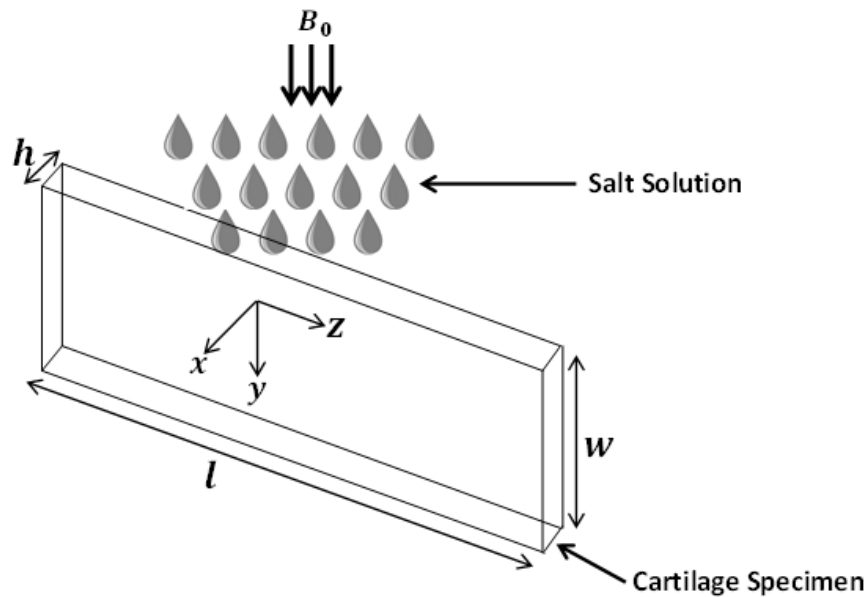


FIGURE 5.1: Schematic diagram and coordinate system of a cartilage specimen under continuous salt bath and magnetic field.

Like other soft biological tissues [17, 28, 75], articular cartilage was also modeled as a mixture composed of porous solid organic matrix and the interstitial fluid [19, 21]. In order to develop the mathematical model, we assume that the fluid is viscous and conducting, solid and fluid are intrinsically incompressible, the elastic solid matrix is linear, homogeneous and isotropic, the viscosity of fluid is negligible except for its contribution to diffusional drag force, osmotic and gravitational forces are neglected and the coefficient of diffusive resistance as well as solid content of the material are independent of deformation. The conservation of mass for the mixture of solid and fluid is written as [21, 76]

$$\operatorname{div} \mathbf{v}^\ell = -\psi \operatorname{div} \mathbf{v}^s, \quad (5.1)$$

where \mathbf{v}^ℓ and \mathbf{v}^s denote the fluid and solid velocity, respectively, and ψ is the ratio of solid to fluid volume. The momentum balance for the solid and fluid phase by taking into account the body force due to magnetic field is given by [69]

$$\rho^\eta \left(\frac{\partial \mathbf{v}^\eta}{\partial t} + (\mathbf{v}^\eta \cdot \nabla) \mathbf{v}^\eta \right) = \nabla \cdot \mathbf{T}^\eta + \rho^\eta \mathbf{b}^\eta + \boldsymbol{\pi}^\eta + \mathbf{J} \times \mathbf{B}, \quad (5.2)$$

where $\eta = s$, represents the solid, and $\eta = \ell$, the fluid phase of the mixture. Here, ρ^η , \mathbf{v}^η , \mathbf{T}^η and $\boldsymbol{\pi}^\eta$ denote respectively the density, velocity, stress and drag force of the η phase whereas \mathbf{J} represents the current density and \mathbf{B} the magnetic flux density. The body force except the magnetic field is neglected here. The inertial terms appearing on the left hand side of equation (5.2) were taken into account for the derivation of governing equations by Barry and Aldis [25] and proven to be negligible for a particular choice of time scale but our reason for neglecting these terms is due to small velocities and deformations that reduces the momentum equation to the following form

$$\nabla \cdot \mathbf{T}^\eta + \boldsymbol{\pi}^\eta + \mathbf{J} \times \mathbf{B} = \mathbf{0}, \quad (5.3)$$

where Newton's third law for the internal frictional forces implies that $\boldsymbol{\pi}^s + \boldsymbol{\pi}^\ell = \mathbf{0}$. Following [69], the Maxwell's equations of electromagnetism along with Ohm's law

can be written as

$$\nabla \times \mathbf{B} = \mu_c \mathbf{J}, \quad \nabla \cdot \mathbf{B} = 0, \quad \nabla \times \mathbf{E} = -\frac{\partial \mathbf{B}}{\partial t}, \quad \mathbf{J} = \sigma_0(\mathbf{E} + \mathbf{v}^\eta \times \mathbf{B}), \quad (5.4)$$

where μ_c is the permeability of free space, \mathbf{E} the electric field and σ_0 the electric conductivity of fluid. The solid stress \mathbf{T}^s and fluid stress \mathbf{T}^ℓ may be defined as [37]

$$\mathbf{T}^s = -\psi p \mathbf{I} + 2\mu \mathbf{e} + \lambda e \mathbf{I} + \psi_c(3\lambda + 2\mu)C \mathbf{I}, \quad (5.5)$$

$$\mathbf{T}^\ell = -p \mathbf{I}. \quad (5.6)$$

Here p is fluid pressure, \mathbf{I} the identity tensor, \mathbf{e} the infinitesimal strain tensor, e the trace of strain tensor, (λ, μ) Lamé stress constants, ψ_c the coefficient of isotropic chemical contraction and C the molar concentration of salt. It is important to note that the last term appearing on right hand side of equation (5.5) represents the contribution of ion concentration in the biphasic modeling of ion-induced deformation. Myers *et al.* [36] considered an exponential form of the chemical expansion stress estimated from experimental data by employing the triphasic mixture theory [33]. However, the biphasic theory with the inclusion of ion concentration term in the solid stress equation, nevertheless, captures the similar dynamics to that of triphasic theory along with the advantage of solving a relatively easier system of equations. The drag force between the constituents is given by [37]

$$-\boldsymbol{\pi}^s = \boldsymbol{\pi}^\ell = K(\mathbf{v}^s - \mathbf{v}^\ell), \quad (5.7)$$

where K is the coefficient of diffusive resistance. Using equations (5.4) and (5.7) into equation (5.3), we obtain for the solid and the fluid phase the following

$$\nabla \cdot \mathbf{T}^s - K(\mathbf{v}^s - \mathbf{v}^\ell) - \sigma_0 B_0^2 \mathbf{v}^s = \mathbf{0}, \quad (5.8)$$

$$\nabla \cdot \mathbf{T}^\ell + K(\mathbf{v}^s - \mathbf{v}^\ell) - \sigma_0 B_0^2 \mathbf{v}^\ell = \mathbf{0}, \quad (5.9)$$

where B_0 is the constant magnetic flux. Note that the last term appearing in equations (5.8) and (5.9) is the contribution of the MHD to the modeling of fluid

flow through a deformable porous material [69]. Incorporation of the stress relations (5.5) and (5.6) into equations (5.8) and (5.9) respectively, yields

$$\begin{aligned} -\psi\nabla p + 2\mu\nabla \cdot \mathbf{e} + \lambda\nabla e + \psi_c(3\lambda + 2\mu)\nabla C - K(\mathbf{v}^s - \mathbf{v}^\ell) \\ -\sigma_0 B_0^2 \mathbf{v}^s = \mathbf{0}, \end{aligned} \quad (5.10)$$

$$-\nabla p + K(\mathbf{v}^s - \mathbf{v}^\ell) - \sigma_0 B_0^2 \mathbf{v}^\ell = \mathbf{0}. \quad (5.11)$$

Elimination of the pressure term from these equations leads to

$$\begin{aligned} -K(1 + \psi)(\mathbf{v}^s - \mathbf{v}^\ell) - \sigma_0 B_0^2(\mathbf{v}^s - \psi\mathbf{v}^\ell) + 2\mu\nabla \cdot \mathbf{e} + \lambda\nabla e + \\ \psi_c(3\lambda + 2\mu)\nabla C = \mathbf{0}. \end{aligned} \quad (5.12)$$

Following Myers *et al.* [37], we assume that the interstitial flow field is one-dimensional and $u(x, t)$ and $v^\ell(x, t)$ denote respectively the solid displacement and fluid velocity component in the thickness direction. Thus, integrating the continuity equation (5.1), we obtain

$$v^\ell = -\psi \frac{\partial u}{\partial t}. \quad (5.13)$$

Keeping in view equation (5.13) and taking the solid velocity component, $v^s = \frac{\partial u}{\partial t}$, we can write equation (5.12) in scalar form as

$$-K(1 + \psi)^2 \frac{\partial u}{\partial t} - \sigma_0 B_0^2(1 + \psi^2) \frac{\partial u}{\partial t} + (\lambda + 2\mu) \frac{\partial^2 u}{\partial x^2} + \psi_c(3\lambda + 2\mu) \frac{\partial C}{\partial x} = 0, \quad (5.14)$$

which can be written after simple mathematical manipulation as

$$\left(\frac{1 + \kappa\sigma_0 B_0^2(1 + \psi^2)}{\kappa} \right) \frac{\partial u}{\partial t} = (\lambda + 2\mu) \frac{\partial^2 u}{\partial x^2} + \psi_c(3\lambda + 2\mu) \frac{\partial C}{\partial x}, \quad (5.15)$$

where

$$\kappa = \frac{1}{K(1 + \psi)^2}, \quad (5.16)$$

is defined as the permeability of the elastic solid matrix. Many authors [24, 64, 77]

have considered different forms of this functional relationship to account for the fluid flow through various porous materials. It appears that the most versatile and commonly used form of permeability in biomechanics is [21]

$$\kappa = \kappa_0 e^{m \frac{du}{dx}}, \quad (5.17)$$

where $\frac{du}{dx}$ is the one-dimensional strain or dilatation and κ_0 and m are material constants. It is important to note that the permeability parameter m lies in the range $0 \leq m \leq 10$ for articular cartilage [78], where $m = 0$ correspond to constant and $m \neq 0$ correspond to nonlinear permeability. Using the relation (5.17) into (5.15) and after simple mathematical manipulation, we obtain

$$\frac{\partial u}{\partial t} = \frac{\kappa_0 e^{m \frac{du}{dx}}}{1 + M e^{m \frac{du}{dx}}} \left(H_a \frac{\partial^2 u}{\partial x^2} + \psi_c E \frac{\partial C}{\partial x} \right), \quad (5.18)$$

where $M = \kappa_0 \sigma_0 B_0^2 (1 + \psi^2)$ is defined to be the dimensionless magnetic parameter, $H_a = (\lambda + 2\mu)$ is the aggregate modulus and $E = 3\lambda + 2\mu$. Equation (5.18) is required governing equation in terms of solid displacement as a function of distance x and time t . The solid displacement may be obtained once the ion concentration $C(x, t)$ in the tissue is known. It is to remark here that setting the magnetic parameter M to zero and considering the permeability to be constant (i.e. $m = 0$ or $\kappa = \kappa_0$) in equation (5.18), we recover the displacement equation in Myers *et al.* [37] in dimensional form. Equation (5.18) is subject to the following initial and boundary conditions

$$u(x, 0) = 0, \quad u(0, t) = 0, \quad \frac{\partial u}{\partial x}(\pm h/2, t) = -\frac{\psi_c E}{H_a} C(\pm h/2, t). \quad (5.19)$$

In order to obtain a relation for the interstitial fluid pressure $p(x, t)$ in the tissue, we combine equations (5.10) and (5.11) to get

$$-(1 + \psi) \nabla p + 2\mu \nabla \cdot \mathbf{e} + \lambda \nabla e + \psi_c (3\lambda + 2\mu) \nabla C - \sigma_0 B_0^2 (\mathbf{v}^s + \mathbf{v}^\ell) = \mathbf{0}. \quad (5.20)$$

Utilizing again the relations $v^\ell = -\psi \frac{\partial u}{\partial t}$ and $v^s = \frac{\partial u}{\partial t}$, we can write equation (5.20) in scalar form as

$$\frac{\partial p}{\partial x} = \frac{H_a}{(1 + \psi)} \frac{\partial^2 u}{\partial x^2} - \frac{\sigma_0 B_0^2 (1 - \psi)}{(1 + \psi)} \frac{\partial u}{\partial t} + \frac{\psi_c E}{(1 + \psi)} \frac{\partial C}{\partial x}. \quad (5.21)$$

Elimination of the term $\frac{\partial u}{\partial t}$ from equations (5.18) and (5.21) gives

$$\begin{aligned} \frac{\partial p}{\partial x} = & \left\{ \frac{H_a}{(1 + \psi)} - \frac{H_a M (1 - \psi) e^{m \frac{du}{dx}}}{(1 + \psi)(1 + \psi^2)(1 + M e^{m \frac{du}{dx}})} \right\} \frac{\partial^2 u}{\partial x^2} + \\ & \left\{ \frac{\psi_c E}{(1 + \psi)} - \frac{\psi_c M E (1 - \psi) e^{m \frac{du}{dx}}}{(1 + \psi)(1 + \psi^2)(1 + M e^{m \frac{du}{dx}})} \right\} \frac{\partial C}{\partial x}, \end{aligned} \quad (5.22)$$

subject to the condition

$$p(\pm h/2, t) = 0. \quad (5.23)$$

Note that equation (5.22) on integration gives the fluid pressure $p(x, t)$ in the tissue once the solid displacement $u(x, t)$ and ion concentration $C(x, t)$ profiles are known. The contribution of the nonlinear permeability in pressure comes from equation for the solid displacement (5.18). Moreover, the second term on the right side of equation (5.21) is the contribution of MHD towards the fluid pressure and setting this term equal to zero recovers the corresponding equation in [37].

In order to complete the dynamical problem under consideration it is now important to state the diffusion problem for the internal salt concentration for articular cartilage. Following Myers *et al.* [37], we suppose that the diffusion problem is uncoupled from the displacement and that the diffusion of salt is unaffected by the convection effect due to fluid flow and body forces. Moreover, because of the thin specimen of the tissue, the diffusion of NaCl in the tissue is assumed to be one-dimensional.

$$\frac{\partial C}{\partial t} = D \frac{\partial^2 C}{\partial x^2}, \quad (5.24)$$

subject to the initial and boundary conditions

$$C(x, 0) = 0, \quad \frac{\partial C}{\partial x}(0, t) = 0, \quad C(\pm h/2, t) = C_0 H(t), \quad (5.25)$$

where D is the diffusion coefficient of salt in the tissue, C_0 the step rise in salt concentration on tissue sample and $H(t)$ the unit step Heaviside function. Note that we use the solution for ion concentration $C(x, t)$ from equations (5.24) and (5.25) in equations (5.18) and (5.21) to get solutions for solid displacement and fluid pressure of porous tissue. Below we present solution methodology for the governing set of partial differential equations.

5.3 Solution Procedure

We introduce the following set of dimensionless quantities to non-dimensionalize the ion concentration, solid displacement and fluid pressure equations

$$\bar{t} = D \frac{t}{(h/2)^2}, \quad \bar{x} = \frac{x}{h/2}, \quad \bar{u} = \frac{u}{h/2}, \quad \bar{C} = \frac{C}{C_0}, \quad \bar{p} = \frac{p}{p_0}, \quad (5.26)$$

where p_0 is a typical pressure scale. The resulting equations on dropping the bars take the following form, i.e. ion concentration

$$\frac{\partial C}{\partial t} = \frac{\partial^2 C}{\partial x^2}, \quad (5.27)$$

$$C(x, 0) = 0, \quad \frac{\partial C}{\partial x}(0, t) = 0, \quad C(\pm 1, t) = H(t), \quad (5.28)$$

which has the following solution

$$C(x, t) = 1 - \frac{4}{\pi} \sum_{k=0}^{\infty} \frac{(-1)^k}{2k+1} \cos\left(\frac{(2k+1)\pi x}{2}\right) e^{-\frac{(2k+1)^2 \pi^2}{4} t}. \quad (5.29)$$

The solid displacement

$$\frac{\partial u}{\partial t} = \frac{R e^{m \frac{du}{dx}}}{1 + M e^{m \frac{du}{dx}}} \left(\frac{\partial^2 u}{\partial x^2} + Q \frac{\partial C}{\partial x} \right), \quad (5.30)$$

$$u(x, 0) = 0, \quad u(0, t) = 0, \quad \frac{\partial u}{\partial x}(\pm 1, t) = -Q. \quad (5.31)$$

where $R = \frac{\kappa_0 H_a}{D}$ and $Q = \frac{\psi_c C_0 E}{H_a}$ are dimensionless parameters. Considering the permeability function to be constant (i.e. $m = 0$) and using the expression (5.29) into equation (5.30), the closed form solution for the solid displacement $u(x, t)$ by employing the eigenfunction expansion method using Green's formula is written as

$$u(x, t) = \frac{8}{\pi^2} \sum_{k=0}^{\infty} \frac{(-1)^k}{(2k+1)^2} \sin\left(\frac{(2k+1)\pi x}{2}\right) \times \left[\frac{RQ}{R-M-1} e^{-\frac{(2k+1)^2 \pi^2 t}{4}} + \frac{Q(1+M)}{M-R+1} e^{-\frac{-R(2k+1)^2 \pi^2 t}{4(1+M)}} - Q \right]. \quad (5.32)$$

The interstitial fluid pressure

$$\frac{\partial p}{\partial x} = \left\{ \frac{H_a}{p_0(1+\psi)} - \frac{H_a M(1-\psi) e^{m \frac{du}{dx}}}{p_0(1+\psi)(1+\psi^2)(1+M e^{m \frac{du}{dx}})} \right\} \frac{\partial^2 u}{\partial x^2} + \left\{ \frac{QH_a}{p_0(1+\psi)} - \frac{QH_a M(1-\psi) e^{m \frac{du}{dx}}}{p_0(1+\psi)(1+\psi^2)(1+M e^{m \frac{du}{dx}})} \right\} \frac{\partial C}{\partial x}, \quad (5.33)$$

$$p(\pm 1, t) = 0, \quad (5.34)$$

whose solution in view of equations (5.29) and (5.32) for $m = 0$ is be written as

$$p(x, t) = \frac{4QH_a(1+M)}{\pi(M-R+1)} \left\{ \frac{1}{p_0(1+\psi)} - \frac{M(1-\psi)}{p_0(1+M)(1+\psi)(1+\psi^2)} \right\} \times \sum_{k=0}^{\infty} \frac{(-1)^k}{2k+1} \cos\left(\frac{(2k+1)\pi x}{2}\right) \times \left[e^{-\frac{-R(2k+1)^2 \pi^2 t}{4(1+M)}} - e^{-\frac{(2k+1)^2 \pi^2 t}{4}} \right]. \quad (5.35)$$

It is important to note that for large times, the steady state solution for concentration and displacement of equations (5.27) and (5.30) reduce to $C_\infty = 1$ and $u_\infty = -Qx$, respectively, which means that a constant concentration and a linear displacement is obtained for steady state case and a similar result was reported in [36] for triphasic theory. Moreover, since the parameter Q is positive, therefore,

the steady state displacement u_∞ will be negative and this suggests that tissue will contract with the passage of time. We now turn our attention to the solution of the nonlinear problem when the permeability parameter $m \neq 0$ in equation (5.30) and hence in equation (5.33). In particular, the closed form solution for the solid displacement and the fluid pressure calculated previously cannot be found due to the nonlinear nature of the partial differential equation. The solution of this problem is computed numerically using method of lines (MOL) technique. For completeness, we now show a brief calculation of the MOL by discretizing the governing equation (5.30) after using equation (5.29) and employing the central finite difference formulas for the space derivatives to give

$$\frac{du_i}{dt} = \frac{R e^{m \frac{u_{i+1} - u_{i-1}}{2dx}}}{1 + M e^{m \frac{u_{i+1} - u_{i-1}}{2dx}}} \times \left[\frac{u_{i+1} - 2u_i + u_{i-1}}{(dx)^2} + 2Q \sum_{k=0}^{\infty} (-1)^k \sin \left(\frac{(2k+1)\pi x_i}{2} \right) e^{-\frac{(2k+1)^2 \pi^2 t}{4}} \right], \quad (5.36)$$

where

$$i = 1, 2, 3, \dots, N, \quad u_i = u(x_i, t), \quad x_i = a + (i - 1)dx, \quad dx = \frac{b - a}{N}. \quad (5.37)$$

From the boundary conditions for the displacement, we have

$$u_0 = 0, \quad u_{N+1} = \frac{1}{3}(-2hQ + 4u_N - u_{N-1}). \quad (5.38)$$

Here a and b denote respectively the left and right end points of the domain and N is the number of spatial nodes. Moreover, u_0 corresponds to the left boundary condition and u_{N+1} represents the approximated right boundary condition [61] of the solid displacement. From the initial condition for the solid displacement, we have

$$u(x_i, 0) = 0. \quad (5.39)$$

Thus, we have an initial value problem consisting of N number of ODEs in equation (5.36) and corresponding initial conditions outlined in equation (5.39) which

may now be solved using efficient Matlab solvers such as *ode23s*. It is important to note that we truncated the temporal domain at $t = 5$ because after this value there is no significant change in the ion concentration and solid displacement distributions and hence the long time behavior of the solutions may be obtained. The pressure gradient in equation (5.33) is solved numerically using the trapezoidal rule for the nonlinear permeability case. A comparison between the exact and numerical solution for the ion concentration profile is presented in Figure 5.2 below. The values of various parameters considered in this chapter are $R = 0.4$, $Q = 0.03630$, $H_a = 4$, $\psi = 0.3$, $p_0 = 1$ and these values are consistent with previous related studies [36, 37].

5.4 Results and Discussion

In this section, we present graphical results for the ion concentration, solid displacement and fluid pressure profiles for articular cartilage as a function of non-dimensional distance and time. In particular, the exact solutions for the constant permeability and numerical solutions obtained for the nonlinear permeability case are discussed to explore the dynamical features caused by the magnetic and permeability parameter.

5.4.1 Ion concentration profile

Figure 5.2 describes ion concentration distribution in the tissue as a function of distance x at time $t = 0.1, 0.25, 1.0, 4.0$. The concentration of the ions in the tissue increases gradually with time due to diffusion process and attains an equilibrium state at time $t = 4$. However, for the triphasic theory [36], the equilibrium value of the ion concentration was reported to be approximately 0.71.

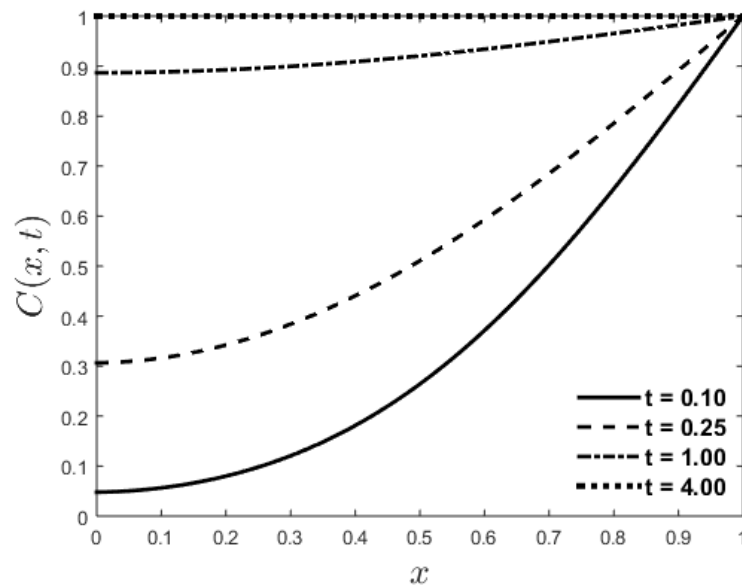


FIGURE 5.2: Ion concentration vs distance at $t = 0.1, 0.25, 1.0, 4.0$.

5.4.2 Influence of magnetic parameter

Figures 5.3, 5.4 and 5.5 describe the effect of magnetic parameter M on solid displacement, fluid pressure and strain-dependent permeability respectively for various times as a function of distance x . In Figure 5.3, solid displacement increases by increasing magnetic parameter from the center line of the tissue with more profound effect for large times. This effect is in accordance with the earlier related study [69] for the fluid flow through a thin deformable porous layer. On the other hand, for the fixed value of the magnetic parameter, the tissue contracts uniformly with the passage of time and follows a linear behavior as an equilibrium state for a long time as validated by equation (5.32). The slope of the final state in the absence of magnetic effects (i.e. $M = 0$), as predicted in [36], is found to be -0.03630 and this slope gets shallower with an increase in the strength of magnetic field. This fact suggests that there could be an expansion of the tissue before final contraction for small times when the applied magnetic field is high.

For the constant permeability case, the interstitial fluid pressure in the tissue increases with magnetic parameter for large times, however, an opposite effect is

noted for small times as shown in Figure 5.4. The fluid pressure vanishes slowly in the presence of MHD effects. Keeping magnetic parameter fixed, the fluid pressure elevates in the tissue for time $t = 0.1$ due to salt-induced contraction of the porous tissue. The subsequent decrease of pressure is caused by the discharge of fluid across the tissue surface. This observation is consistent with [37] when magnetic effects are absent.

The strain-dependent permeability κ under a chemical expansion stress in Figure 5.5 is observed to increase with the increase in magnetic parameter with dominant effect for large time. This means that a high magnetic field would allow more fluid to pass through the tissue and this effect can be utilized for clinical purposes which need to be explored in more details. Interestingly, when stress is relaxed the concentration, displacement and pressure distributions in Figures 5.2, 5.3 and 5.4 respectively, appear to achieve the equilibrium states when the magnetic effects are absent.

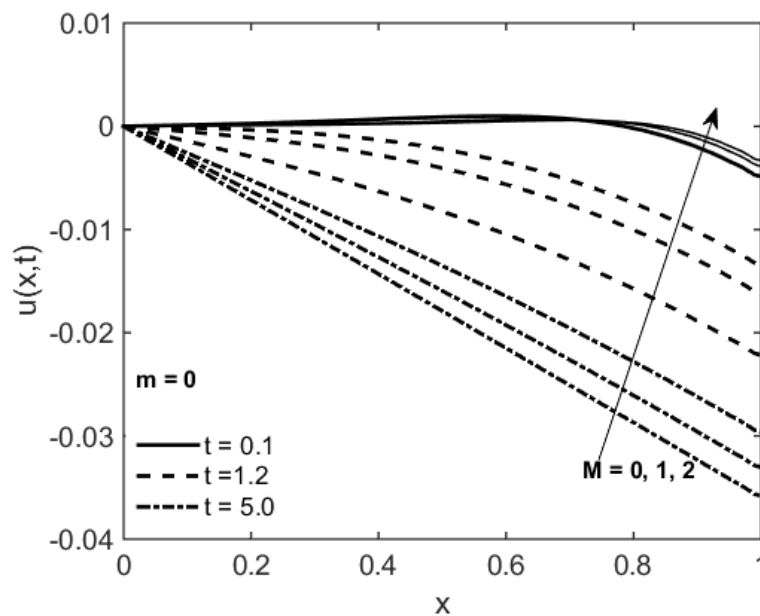


FIGURE 5.3: Solid displacement vs distance for various M at $t = 0.1, 1.2, 5.0$ when $m = 0$.

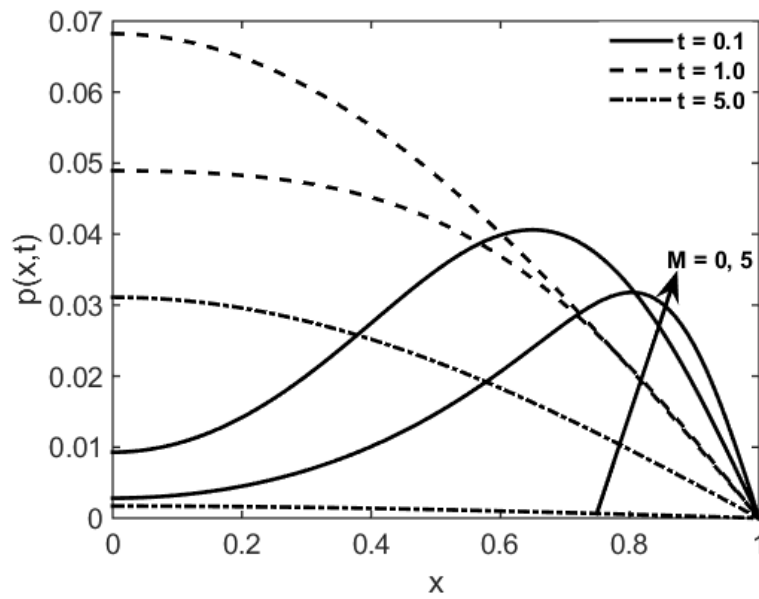


FIGURE 5.4: Fluid pressure vs distance for various M at $t = 0.1, 1.0, 5.0$ when $m = 0$.

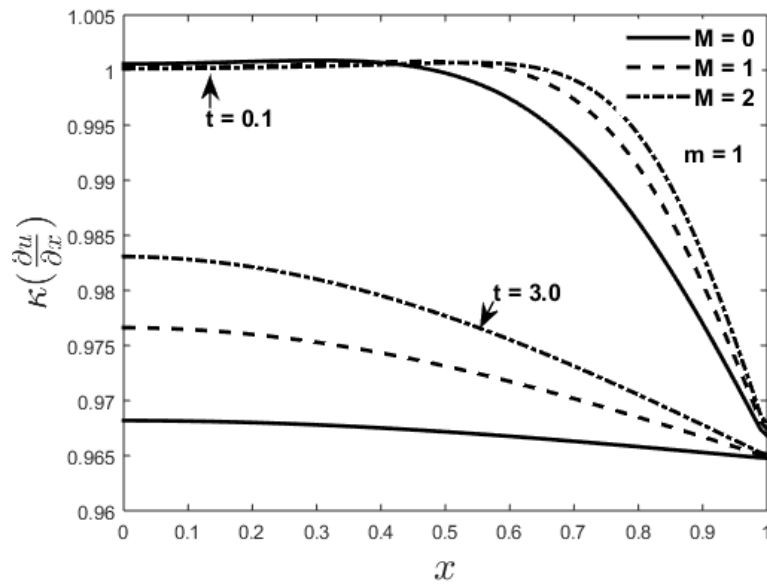


FIGURE 5.5: Strain-dependent permeability vs distance for various M at $t = 0.1, 3.0$ when $m = 1.0$.

5.4.3 Influence of permeability parameter

The solid displacement and pressure gradient profiles are plotted as a function of distance and time for various values of permeability parameter m in Figures 5.6

and 5.7, respectively. In Figure 5.6, solid displacement increases, although slightly, with permeability parameter for small as well as large time. This means that the tissue will experience a contraction with a decrease in permeability parameter. Indeed, due to negative chemical expansion stress and zero initial concentration and displacement conditions, the subsequent deformations are contractions and displacement u must be negative as predicted. Moreover, the effect of permeability parameter on solid displacement is consistent with previous related studies [24, 53] on flow-induced deformation in porous biological tissues.

The pressure gradient profile $\frac{\partial p}{\partial x}$ in Figure 5.7 appears to decrease with an increase in permeability parameter for a fixed distance from the center line of the rectangular sample of tissue, however as before, an opposite trend is observed for smaller values of time. This suggests that fluid pressure in the tissue would increase with permeability parameter and this result is also consistent with previous studies [24, 53], the difference, of course, is the geometry and the presence of chemical effects here. The pressure gradient at large times is negative suggesting that the interstitial fluid pressure is a decreasing function of time for the nonlinear permeability as well.

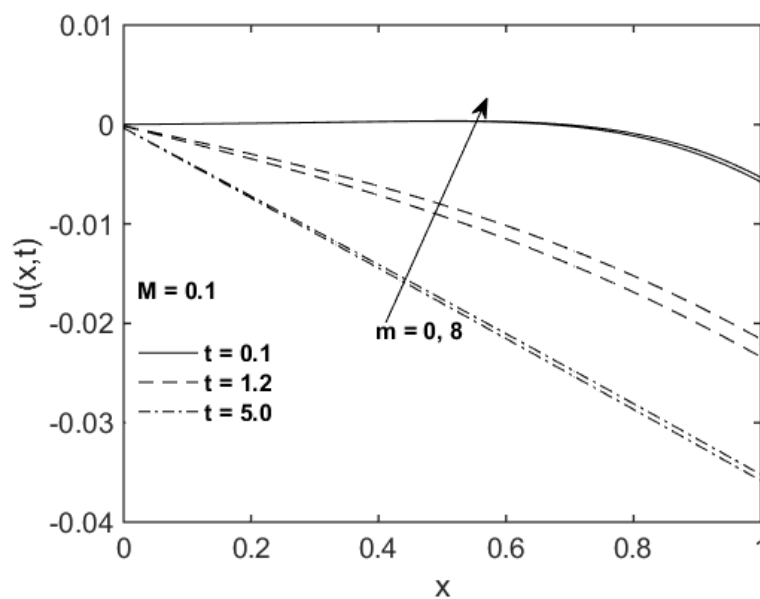


FIGURE 5.6: Solid displacement vs distance for various m at $t = 0.1, 1.2, 5.0$ when $M = 0.1$.

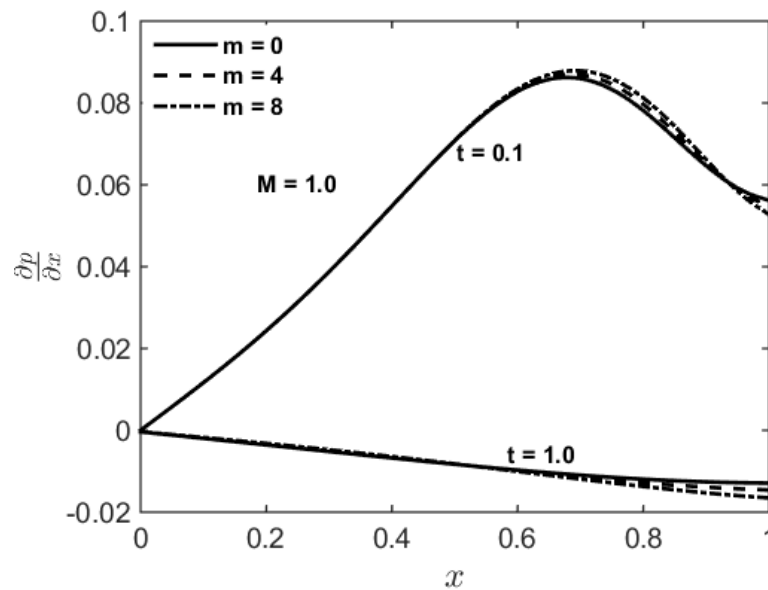


FIGURE 5.7: Pressure gradient vs distance for various m at $t = 0.1, 1.0$ when $M = 1.0$.

5.5 Concluding Remarks

We have examined ion-induced deformation of articular cartilage with strain-dependent nonlinear permeability and magnetohydrodynamics (MHD) effects. In particular, a thin rectangular specimen of bovine cartilage was exposed to a uniform applied magnetic field and allowed to swell freely under a continuous salt shower. We used a biphasic mixture theory with the inclusion of ion concentration term in the solid stress equation. A one-dimensional PDE uncoupled from the solid displacement was considered to account for the salt diffusion in the porous tissue.

The solid displacement and fluid pressure in articular cartilage were found to increase as the strength of the externally applied magnetic field was increased, however, an opposite effect was noted for a small time. This solid deformation allows more fluid to pass through the tissue which enhances the fluid pressure in the tissue. This effect may be of importance in some physiological processes. It was also noted that the application of a high magnetic field may cause the tissue

to expand for a specified time before final contraction due to chemical expansion stress. Like the magnetic parameter, solid displacement and fluid pressure were also found to increase with an increase in the permeability parameter, however, the effect was not that apparent. Moreover, the presence of magnetohydrodynamics effects elevated the strain-dependent permeability, particularly, for large time. Finally, it is worth mentioning that the influence of magnetic parameter on steady-state solutions was absent.

This work contributes to enhancing the understanding of the behavior of articular cartilage under the action of an applied magnetic field. This study is also relevant to the situations where the electric or the magnetic energy is generated with the help of an electronic device outside excitable tissues including articular cartilage to activate and magnetize the tissues for clinical purposes. The findings of the current research suggest that this mathematical model may further be improved both theoretically and experimentally.

Chapter 6

Conclusion and Future Work

In this dissertation, a number of problems related to fluid flow through deformable porous biological tissues are considered. A continuum mixture theory approach is used to model these problems. Below we conclude the present study and indicate some possible future directions.

6.1 Conclusion

Over the past forty years, there is a tremendous rise in the interest to examine the fluid flow through rigid as well as deformable porous media. However, special attention has been given to mathematical modeling of the biological problems where many soft tissues exhibit deformable porous behavior and applications of mixture theory becomes a natural need. By using a biphasic mixture theory, the problems of flow and ion-induced deformation of soft porous tissues are modeled in this thesis. Partial differential equations for the fluid pressure and the solid displacement are obtained by using the fundamental laws of conservation of mass and linear momentum. These PDEs are non-dimensionalized by using the appropriate dimensionless variables and the emerging non-dimensional parameters are also defined. The governing equations are solved analytically as well as numerically and the solutions are illustrated graphically. In some cases, the results are

also compared with those of the previously published papers. The main findings of the present research have been listed as below.

1. It is observed that the flow-induced deformation improves the fluid absorption in the tissue.
2. The porosity of the medium is increased due to annular expansion of the porous tissue.
3. It is noted that the shear-thinning fluids exhibit greater fluid pressure and solid deformation in the tissue as compared to the shear-thickening fluids.
4. The effect of nonlinearities is observed to be more significant for the shear-thinning fluids than the Newtonian and shear-thickening fluids.
5. The power-law fluid pressure and solid displacement are decreased by increasing the permeability and absorption parameter.
6. A considerable reduction in the permeability of the porous tissue is noted in the presence of rheological effects.
7. The solid deformation enhances the permeability of the medium which results in an increment in the local porosity of the tissue.
8. A reasonable reduction in the fluid pressure and the solid displacement of the spherical cavity is observed in the presence of the magnetic effects.
9. The magnetic parameter does not affect the steady-state solutions.
10. The concentration of ions in articular cartilage is increased gradually with time and an equilibrium state is achieved for $t \geq 4$.
11. In general, the displacement of the solid and fluid pressure in articular cartilage is found to increase as the strength of the externally applied magnetic field is increased.
12. A high magnetic field allows the cartilage to expand for a short interval of time before the final contraction.

13. Importantly, the deformation of the cartilage allows more fluid to seep through it which results in an increment in the fluid pressure.
14. An enhancement in the permeability parameter results into an increment in the solid displacement and the fluid pressure in the articular cartilage.

6.2 Future Work

The continuum mixture theory has already been used successfully for a number of problems in physics and biology. In the present work by using this theory, some unresolved problems in biomechanics are addressed. However, there is still a need to further improve the modeling of the real life problems in this area. Some interesting possible questions that have not been addressed yet and could be investigated in future are listed below.

1. The effect of non-Newtonian magnetohydrodynamics fluid on flow-induced deformation of absorbing porous tissues can be considered.
2. The non-Newtonian modeling of ion-induced deformation of articular cartilage may be undertaken.
3. In modeling the problems in this thesis, we assumed that tissues are homogeneous and isotropic, however, in-homogeneity and anisotropy of the tissues can also be considered for more accurate modeling.
4. Consideration of nonlinear stress-strain relationship, different permeability functions, sophisticated chemical stress mechanism, and more realistic geometries can enhance the understanding of the solid-fluid interaction in soft tissues.
5. Analysis of full nonlinear moving boundary value problem along with variable magnetic field can also be investigated.

6. A more sophisticated form of the absorption process in the tissues and refined forms of the drag force between the constituents of the mixture can be considered.
7. Another interesting future direction could be the consideration of more realistic fluid models along with appropriate boundary conditions.
8. Last but not the least, the models presented in this thesis are based on the theory, however, experiments can be undertaken to validate and improve these models for physiological as well as clinical applications.

Bibliography

- [1] J. D. Humphrey, “Continuum biomechanics of soft biological tissues,” *Proceedings of the Royal Society of London A: Mathematical, Physical and Engineering Sciences*, vol. 459, no. 2029, pp. 3–46, 2003.
- [2] J. I. Siddique, A. Ahmed, A. Aziz, and C. M. Khalique, “A review of mixture theory for deformable porous media and applications,” *Applied Sciences*, vol. 7, no. 9, pp. 917–931, 2017.
- [3] A. Fick, “Ueber diffusion,” *Annalen der Physik*, vol. 170, no. 1, pp. 59–86, 1855.
- [4] J. Stefan, “Über das gleichgewicht and die bewegung insbesondere die diffusion von gasmenger,” *Sitzungsberichte der Kaiserlichen Akademie der Wissenschaften*, vol. 63, pp. 63–124, 1871.
- [5] W. Darcy, “Continuum mixture theory,” *ZAMM Journal of Applied Mathematics and Mechanics*, vol. 1, pp. 121–151, 1851.
- [6] C. Truesdell and W. Noll, “The non-linear field theories of mechanics,” in *The Non-linear Field Theories of Mechanics*. Springer, 2004, pp. 1–579.
- [7] I. Müller, “A thermodynamic theory of mixtures of fluids,” *Archive for Rational Mechanics and Analysis*, vol. 28, no. 1, pp. 1–39, 1968.
- [8] R. Atkin and R. Craine, “Continuum theories of mixtures: basic theory and historical development,” *The Quarterly Journal of Mechanics and Applied Mathematics*, vol. 29, no. 2, pp. 209–244, 1976.

-
- [9] R. M. Bowen, *Theory of Mixtures. In Continuum Physics (ed. A. C. Eringen)*. Academic, 1976, vol. 1.
- [10] A. Bedford and D. S. Drumheller, "Theories of immiscible and structured mixtures," *International Journal of Engineering Science*, vol. 21, no. 8, pp. 863–960, 1983.
- [11] K. R. Rajagopal and L. Tao, *Mechanics of Mixtures*. World scientific, 1995, vol. 35.
- [12] D. E. Kenyon, "The theory of an incompressible solid-fluid mixture," *Archive for Rational Mechanics and Analysis*, vol. 62, no. 2, pp. 131–147, 1976.
- [13] —, "Transient filtration in a porous elastic cylinder," *ASME Journal of Applied Mechanics*, vol. 43, no. 4, pp. 594–598, 1976.
- [14] —, "Consolidation in compressible mixtures," *Journal of Applied Mechanics*, vol. 45, no. 4, p. 727, 1978.
- [15] G. Jayaraman, "Water transport in the arterial wall a theoretical study," *Journal of Biomechanics*, vol. 16, no. 10, pp. 833–840, 1983.
- [16] R. Jain and G. Jayaraman, "A theoretical model for water flux through the artery wall," *Journal of Biomechanical Engineering*, vol. 109, no. 4, p. 311, 1987.
- [17] M. Klanchar and J. Tarbell, "Modeling water flow through arterial tissue," *Bulletin of Mathematical Biology*, vol. 49, no. 6, pp. 651–669, 1987.
- [18] V. C. Mow and W. M. Lai, "Mechanics of animal joints," *Annual Review of Fluid Mechanics*, vol. 11, no. 1, pp. 247–288, 1979.
- [19] V. C. Mow, M. H. Holmes, and W. M. Lai, "Fluid transport and mechanical properties of articular cartilage: a review," *Journal of Biomechanics*, vol. 17, no. 5, pp. 377–394, 1984.

- [20] V. C. Mow and J. M. Mansour, "The nonlinear interaction between cartilage deformation and interstitial fluid flow," *Journal of Biomechanics*, vol. 10, no. 1, pp. 31–39, 1977.
- [21] W. M. Lai and V. C. Mow, "Drag-induced compression of articular cartilage during a permeation experiment," *Biorheology*, vol. 17, no. 1-2, pp. 111–123, 1980.
- [22] S. Kuei, W. M. Lai, and V. C. Mow, "A biphasic rheological model of articular cartilage," *Advances in Bioengineering, AH Burstein, ed., ASME, New York*, pp. 17–18, 1978.
- [23] G. Ateshian, H. Wang, and W. M. Lai, "The role of interstitial fluid pressurization and surface porosities on the boundary friction of articular cartilage," *Journal of Tribology*, vol. 120, no. 2, pp. 241–248, 1998.
- [24] S. I. Barry and G. K. Aldis, "Flow-induced deformation from pressurized cavities in absorbing porous tissues," *Bulletin of Mathematical Biology*, vol. 54, no. 6, pp. 977–997, 1992.
- [25] ———, "Comparison of models for flow induced deformation of soft biological tissue," *Journal of Biomechanics*, vol. 23, no. 647-654, pp. 1–20, 1990.
- [26] S. I. Barry, K. H. Parkerf, and G. K. Aldis, "Fluid flow over a thin deformable porous layer," *Zeitschrift für Angewandte Mathematik und Physik (ZAMP)*, vol. 42, no. 5, pp. 633–648, 1991.
- [27] M. Friedman, "General theory of tissue swelling with application to the corneal stroma," *Journal of Theoretical Biology*, vol. 30, no. 1, pp. 93–109, 1971.
- [28] C. Oomens, D. Van Campen, and H. Grootenboer, "A mixture approach to the mechanics of skin," *Journal of Biomechanics*, vol. 20, no. 9, pp. 877–885, 1987.

-
- [29] T. Ford, J. Sachs, J. Grotberg, and M. Glucksberg, “Mechanics of the perialveolar interstitium of the lung,” in *First World Congress of Biomechanics, La Jolla*, vol. 1, 1990, p. 31.
- [30] T. Lekszycki and F. Dell’Isola, “A mixture model with evolving mass densities for describing synthesis and resorption phenomena in bones reconstructed with bio-resorbable materials,” *ZAMM-Journal of Applied Mathematics and Mechanics/Zeitschrift für Angewandte Mathematik und Mechanik*, vol. 92, no. 6, pp. 426–444, 2012.
- [31] I. Giorgio, U. Andreaus, D. Scerrato, and F. Dell’Isola, “A visco-poroelastic model of functional adaptation in bones reconstructed with bio-resorbable materials,” *Biomechanics and Modeling in Mechanobiology*, vol. 15, no. 5, pp. 1325–1343, 2016.
- [32] W. M. Lai, J. Hou, and V. C. Mow, “A triphasic theory for the swelling properties of hydrated charged soft biological tissues,” in *Biomechanics of Diarthrodial Joints*. Springer, 1990, pp. 283–312.
- [33] —, “A triphasic theory for the swelling and deformation behaviors of articular cartilage,” *Journal of Biomechanical Engineering*, vol. 113, no. 3, pp. 245–258, 1991.
- [34] W. Gu, W. M. Lai, and V. C. Mow, “A triphasic analysis of negative osmotic flows through charged hydrated soft tissues,” *Journal of Biomechanics*, vol. 30, no. 1, pp. 71–78, 1997.
- [35] D. Sun, W. Gu, X. Guo, W. M. Lai, and V. C. Mow, “A mixed finite element formulation of triphasic mechano-electrochemical theory for charged, hydrated biological soft tissues,” *International Journal for Numerical Methods in Engineering*, vol. 45, no. 10, pp. 1375–1402, 1999.
- [36] T. Myers, G. Aldis, and S. Naili, “Ion induced deformation of soft tissue,” *Bulletin of Mathematical Biology*, vol. 57, no. 1, pp. 77–98, 1995.

- [37] E. Myers, W. M. Lai, and V. C. Mow, “A continuum theory and an experiment for the ion-induced swelling behavior of articular cartilage,” *Journal of Biomechanical Engineering*, vol. 106, no. 2, pp. 151–158, 1984.
- [38] W. Gu, W. M. Lai, and V. C. Mow, “A mixture theory for charged-hydrated soft tissues containing multi-electrolytes: passive transport and swelling behaviors,” *Journal of Biomechanical Engineering*, vol. 120, no. 2, pp. 169–180, 1998.
- [39] T. Ricken, A. Schwarz, and J. Bluhm, “A triphasic theory for growth in biological tissue—basics and applications,” *Materialwissenschaft und Werkstofftechnik*, vol. 37, no. 6, pp. 446–456, 2006.
- [40] W. Gu, W. M. Lai, and V. C. Mow, “Generalized triphasic theory for multi-electrolyte transport in charged hydrated soft tissues,” in *Proceedings of the 1994 International Mechanical Engineering Congress and Exposition*. ASME, 1994.
- [41] A. J. H. Frijns, J. Huyghe, and J. D. Janssen, “A validation of the quadriphasic mixture theory for intervertebral disc tissue,” *International Journal of Engineering Science*, vol. 35, no. 15, pp. 1419–1429, 1997.
- [42] C. Cyron and J. Humphrey, “Growth and remodeling of load-bearing biological soft tissues,” *Meccanica*, vol. 52, no. 3, pp. 645–664, 2017.
- [43] M. Latorre and J. D. Humphrey, “A mechanobiologically equilibrated constrained mixture model for growth and remodeling of soft tissues,” *ZAMM—Journal of Applied Mathematics and Mechanics/Zeitschrift für Angewandte Mathematik und Mechanik*, 2018.
- [44] Y. Lanir, “Multi-scale structural modeling of soft tissues mechanics and mechanobiology,” *Journal of Elasticity*, vol. 129, no. 1-2, pp. 7–48, 2017.
- [45] T. J. Truster and A. Masud, “A unified mixture formulation for density and volumetric growth of multi-constituent solids in tissue engineering,” *Computer Methods in Applied Mechanics and Engineering*, vol. 314, pp. 222–268, 2017.

-
- [46] M. Pourjafar, B. Taghilou, S. Taghavi, and K. Sadeghy, “On the use of biphasic mixture theory for investigating the linear stability of viscous flow through a channel lined with a viscoelastic porous bio-material,” *International Journal of Non-Linear Mechanics*, 2018.
- [47] H. Byrne and L. Preziosi, “Modelling solid tumour growth using the theory of mixtures,” *Mathematical Medicine and Biology*, vol. 20, no. 4, pp. 341–366, 2003.
- [48] D. Ambrosi and L. Preziosi, “On the closure of mass balance models for tumor growth,” *Mathematical Models and Methods in Applied Sciences*, vol. 12, no. 05, pp. 737–754, 2002.
- [49] L. Preziosi and G. Vitale, “A multiphase model of tumor and tissue growth including cell adhesion and plastic reorganization,” *Mathematical Models and Methods in Applied Sciences*, vol. 21, no. 09, pp. 1901–1932, 2011.
- [50] L. Preziosi, *Cancer Modelling and Simulation*. CRC Press, 2003.
- [51] D. Ambrosi, L. Preziosi, and G. Vitale, “The insight of mixtures theory for growth and remodeling,” *Zeitschrift für angewandte Mathematik und Physik (ZAMP)*, vol. 61, no. 1, pp. 177–191, 2010.
- [52] G. Ateshian and J. Humphrey, “Continuum mixture models of biological growth and remodeling: past successes and future opportunities,” *Annual Review of Biomedical Engineering*, vol. 14, pp. 97–111, 2012.
- [53] A. Ahmed, J. I. Siddique, and A. Mahmood, “Non-newtonian flow-induced deformation from pressurized cavities in absorbing porous tissues,” *Computer Methods in Biomechanics and Biomedical Engineering*, vol. 20, no. 13, pp. 1464–1473, 2017.
- [54] B. Lagree, “Modelling of two-phase flow in porous media with volume-of-fluid method,” Ph.D. dissertation, Paris 6, 2014.

- [55] H. I. Andersson and F. Irgens, “Gravity-driven laminar film flow of power-law fluids along vertical walls,” *Journal of Non-Newtonian Fluid Mechanics*, vol. 27, no. 2, pp. 153–172, 1988.
- [56] M. L. Bansal, *Magneto Therapy*. Jain Publisher, New Delhi, 1976.
- [57] “Pinterest,” <https://www.pinterest.com/pin/590816044836974215/>, accessed: 2018-02-10.
- [58] M. Epstein, *The Elements of Continuum Biomechanics*. John Wiley & Sons, 2012.
- [59] L. Fusi, A. Farina, and D. Ambrosi, “Mathematical modeling of a solid–liquid mixture with mass exchange between constituents,” *Mathematics and Mechanics of Solids*, vol. 11, no. 6, pp. 575–595, 2006.
- [60] W. E. Schiesser and G. W. Griffiths, *A Compendium of Partial Differential Equation Models: Method of Lines Analysis with Matlab*. Cambridge University Press, 2009.
- [61] R. E. White and V. R. Subramanian, *Computational Methods in Chemical Engineering with Maple*. Springer Science & Business Media, 2010.
- [62] R. S. Esfandiari, *Numerical Methods for Engineers and Scientists using MATLAB®*. CRC Press, 2017.
- [63] A. D. Polyanin and V. F. Zaitsev, *Handbook of Nonlinear Partial Differential Equations*. CRC press, 2004.
- [64] J. I. Siddique and D. Anderson, “Capillary rise of a non-newtonian liquid into a deformable porous material,” *Journal of Porous Media*, vol. 14, no. 12, 2011.
- [65] S. I. Barry and G. K. Aldis, “Unsteady flow induced deformation of porous materials,” *International Journal of Non-Linear Mechanics*, vol. 26, no. 5, pp. 687–699, 1991.

- [66] ———, “Radial flow through deformable porous shells,” *Journal of Australian Mathematical Society Series B*, vol. 34, pp. 333–354, 1993.
- [67] J. I. Siddique, D. Anderson, and A. Bondarev, “Capillary rise of a liquid into a deformable porous material,” *Physics of Fluids*, vol. 21, no. 1, p. 013106, 2009.
- [68] J. Hou, M. Holmes, W. M. Lai, and V. C. Mow, “Boundary conditions at the cartilage-synovial fluid interface for joint lubrication and theoretical verifications,” *Journal of Biomechanical Engineering*, vol. 111, no. 1, pp. 78–87, 1989.
- [69] N. T. Eldabe, G. Saddeek, and K. Elagamy, “Magnetohydrodynamic flow of a biviscosity fluid through porous medium in a layer of deformable material,” *Journal of Porous Media*, vol. 14, no. 3, 2011.
- [70] J. I. Siddique and A. Kara, “Capillary rise of magnetohydrodynamics liquid into deformable porous material.” *Journal of Applied Fluid Mechanics*, vol. 9, no. 6, 2016.
- [71] M. H. Holmes, “Comparison theorems and similarity solution approximations for a nonlinear diffusion equation arising in the study of soft tissue,” *SIAM Journal on Applied Mathematics*, vol. 44, no. 3, pp. 545–556, 1984.
- [72] M. Abramowitz and I. A. Stegun, *Handbook of Mathematical Functions: with Formulas, Graphs, and Mathematical Tables*. Courier Corporation, 1964, vol. 55.
- [73] W. E. Schiesser, *The Numerical Method of Lines: Integration of Partial Differential Equations*. Elsevier, 2012.
- [74] A. Farina, P. Cocito, and G. Boretto, “Flow in deformable porous media: modelling and simulations of compression moulding processes,” *Mathematical and Computer Modelling*, vol. 26, no. 11, pp. 1–15, 1997.
- [75] D. E. Kenyon, “A mathematical model of water flux through aortic tissue,” *Bulletin of Mathematical Biology*, vol. 41, no. 1, pp. 79–90, 1979.

-
- [76] M. K. Kwan, W. M. Lai, and V. C. Mow, “A finite deformation theory for cartilage and other soft hydrated connective tissues. equilibrium results,” *Journal of Biomechanics*, vol. 23, no. 2, pp. 145–155, 1990.
- [77] M. H. Holmes, “A nonlinear diffusion equation arising in the study of soft tissue,” *Quarterly of Applied Mathematics*, vol. 41, no. 2, pp. 209–220, 1983.
- [78] V. C. Mow, M. Kwan, W. M. Lai, and M. Holmes, “A finite deformation theory for nonlinearly permeable soft hydrated biological tissues,” in *Frontiers in Biomechanics*. Springer, 1986, pp. 153–179.
- [79] V. J. Rossow, “On flow of electrically conducting fluids over a flat plate in the presence of a transverse magnetic field,” 1958.
- [80] A. Hussanan, Z. Ismail, I. Khan, A. G. Hussein, and S. Shafie, “Unsteady boundary layer mhd free convection flow in a porous medium with constant mass diffusion and newtonian heating,” *The European Physical Journal Plus*, vol. 129, no. 3, p. 46, 2014.

Appendix A

MHD Equations for a Biphasic Mixture

We consider the porous deformable material as a continuous binary mixture of intrinsic incompressible solid and magnetic fluid phase, where each point in the mixture is occupied by both the fluid and the isotropic solid. Balance of mass for the solid and fluid phase can be written as [24]

$$\frac{\partial \rho^s}{\partial t} + \nabla \cdot (\rho^s \mathbf{v}^s) = 0, \quad (\text{A.1})$$

$$\frac{\partial \rho^\ell}{\partial t} + \nabla \cdot (\rho^\ell \mathbf{v}^\ell) = -\beta p, \quad (\text{A.2})$$

where $\mathbf{v}^s, \mathbf{v}^\ell$ are velocities and ρ^s, ρ^ℓ are densities of the solid and fluid phase, respectively, p is the fluid pressure and β a proportionality constant.

Conservation of linear momentum for both phases is written as [69]

$$\rho^\eta \left(\frac{\partial \mathbf{v}^\eta}{\partial t} + (\mathbf{v}^\eta \cdot \nabla) \mathbf{v}^\eta \right) = \nabla \cdot \mathbf{T}^\eta + \rho^\eta \mathbf{b}^\eta + \boldsymbol{\pi}^\eta + \mathbf{J} \times \mathbf{B}, \quad (\text{A.3})$$

where $\eta = s, \ell$ represents either the solid or fluid phase, $\mathbf{T}^\eta = -\phi^\eta p \mathbf{I} + \boldsymbol{\sigma}^\eta$ is the stress tensor for the η phase and $-\boldsymbol{\pi}^s = \boldsymbol{\pi}^\ell = K(\mathbf{v}^s - \mathbf{v}^\ell) - p \nabla \phi^s$ is the friction force term which satisfies the relation $\boldsymbol{\pi}^s + \boldsymbol{\pi}^\ell = \mathbf{0}$. Here \mathbf{I} is the identity tensor, ϕ^η the volume fraction, $\boldsymbol{\sigma}^\eta$ the stress and K the drag coefficient of relative motion.

Moreover, \mathbf{b}^η is the net body force in which the gravitational force is neglected, \mathbf{J} is the current density and \mathbf{B} the magnetic flux density.

Maxwell's equations of electromagnetism along with Ohm's law are written as [69, 70]

$$\nabla \times \mathbf{B} = \mu_c \mathbf{J}, \quad \nabla \cdot \mathbf{B} = 0, \quad \nabla \times \mathbf{E} = -\frac{\partial \mathbf{B}}{\partial t}, \quad \mathbf{J} = \sigma_0(\mathbf{E} + \mathbf{v}^\eta \times \mathbf{B}), \quad (\text{A.4})$$

where μ_c is the permeability of free space, \mathbf{E} the electric field and σ_0 the electric conductivity of the fluid. The Lorentz force term $\mathbf{J} \times \mathbf{B}$ in the momentum equation (A.3) may be written in view of Ohm's law as

$$\mathbf{J} \times \mathbf{B} = \sigma_0(\mathbf{E} + \mathbf{v}^\eta \times \mathbf{B}) \times \mathbf{B}, \quad (\text{A.5})$$

where the total magnetic field \mathbf{B} may be decomposed as [79, 80], $\mathbf{B} = \mathbf{B}_0 + \mathbf{b}$, in which \mathbf{B}_0 is the imposed magnetic field and \mathbf{b} is the induced magnetic field which may be ignored on account of low magnetic field Reynolds number approximation. Thus, equation (A.5) when induced magnetic and electric fields are negligible, takes the form

$$\mathbf{J} \times \mathbf{B} = \sigma_0(\mathbf{v}^\eta \times \mathbf{B}_0) \times \mathbf{B}_0, \quad (\text{A.6})$$

which on using the vector relation $(\mathbf{X} \times \mathbf{Y}) \times \mathbf{Z} = \mathbf{Y}(\mathbf{X} \cdot \mathbf{Z}) - \mathbf{X}(\mathbf{Y} \cdot \mathbf{Z})$, reduces to

$$\mathbf{J} \times \mathbf{B} = \sigma_0 \left(\mathbf{B}_0(\mathbf{v}^\eta \cdot \mathbf{B}_0) - \mathbf{v}^\eta(\mathbf{B}_0 \cdot \mathbf{B}_0) \right). \quad (\text{A.7})$$

Assuming that magnetic field lines are perpendicular to the velocity vector (i.e. $\mathbf{v}^\eta \cdot \mathbf{B}_0 = 0$) and $\mathbf{B}_0 = (0, B_0, 0)$, where B_0 is the strength of the applied magnetic field \mathbf{B}_0 , we have from equation (A.7)

$$\mathbf{J} \times \mathbf{B} = -\sigma_0 B_0^2 \mathbf{v}^\eta. \quad (\text{A.8})$$

Finally, the momentum equation (A.3) takes the following form

$$\rho^n \left(\frac{\partial \mathbf{v}^n}{\partial t} + (\mathbf{v}^n \cdot \nabla) \mathbf{v}^n \right) = \nabla \cdot \mathbf{T}^n + \rho^n \mathbf{b}^n + \boldsymbol{\pi}^n - \sigma_0 B_0^2 \mathbf{v}^n. \quad (\text{A.9})$$

We now turn our attention to the motion of the solid phase. Under the assumptions of small deformations and one-dimensional radial flow, the components of the stress tensor for the solid phase are defined as [24]

$$\sigma_{rr} = (\lambda + 2\mu) \frac{\partial u}{\partial r} + 2\lambda \frac{u}{r}, \quad (\text{A.10})$$

$$\sigma_{\theta\theta} = (\lambda + 2\mu) \frac{u}{r} + \lambda \frac{\partial u}{\partial r} + \lambda \frac{u}{r} = \sigma_{\phi\phi}, \quad (\text{A.11})$$

where λ and μ are Lamé stress constants and all other stress components are assumed to be zero. The divergence of the stress in the radial direction is given by

$$(\nabla \cdot \boldsymbol{\sigma})_r = \frac{\partial \sigma_{rr}}{\partial r} + 2 \frac{\sigma_{rr} - \sigma_{\theta\theta}}{r}. \quad (\text{A.12})$$

Substituting equations (A.10) and (A.11) into equation (A.12) and simplifying, we obtain

$$(\nabla \cdot \boldsymbol{\sigma})_r = H_a \frac{\partial \phi}{\partial r}, \quad (\text{A.13})$$

where

$$\phi = \frac{1}{r^2} \frac{\partial}{\partial r} (r^2 u), \quad (\text{A.14})$$

is the local change in porosity and $H_a = \lambda + 2\mu$ is the aggregate modulus.